

# Antarctic palaeotopography



Guy J. G. Paxman<sup>1,2</sup>

<sup>1</sup>Department of Geography, Durham University, Durham, UK

<sup>2</sup>Lamont-Doherty Earth Observatory, Columbia University, New York, USA

0000-0003-1787-7442

[gpaxman@ldeo.columbia.edu](mailto:gpaxman@ldeo.columbia.edu)

**Abstract:** The development of a robust understanding of the response of the Antarctic Ice Sheet to present and projected future climatic change is a matter of key global societal importance. Numerical ice sheet models that simulate future ice sheet behaviour are typically evaluated with recourse to how well they reproduce past ice sheet behaviour, which is constrained by the geological record. However, subglacial topography, a key boundary condition in ice sheet models, has evolved significantly throughout Antarctica's glacial history. Since mantle processes play a fundamental role in the generation and modification of topography over geological timescales, an understanding of the interactions between the Antarctic mantle and palaeotopography is crucial for developing more accurate simulations of past ice sheet dynamics. This chapter provides a review of the influence of the Antarctic mantle on the long-term evolution of the subglacial landscape, through processes including structural inheritance, flexural isostatic adjustment, lithospheric cooling and thermal subsidence, volcanism and dynamic topography. The uncertainties associated with reconstructing these processes through time are discussed, as are important directions for future research and the implications of the evolving subglacial topography for the response of the Antarctic Ice Sheet to climatic and oceanographic change.

## Overview

### *Unveiling the subglacial landscape of Antarctica*

Antarctica is unique among Earth's continents in that the crust is almost entirely capped by a layer of ice up to 4 km thick. Today, *c.* 99.8% of the Antarctic landmass is concealed beneath the Antarctic Ice Sheet (AIS) (Burton-Johnson *et al.* 2016), and this figure was likely even larger during recent glacial maxima (Bentley *et al.* 2014). The near-total lack of exposure of the Antarctic 'land surface' presents major challenges for understanding the long-term history of the AIS.

The progressive mapping of Antarctica's subglacial topography has been driven by a substantial community effort since the 1970s (Drewry 1983; Lythe *et al.* 2001; Fretwell *et al.* 2013; Morlighem *et al.* 2020; Schroeder *et al.* 2019). Ground-based and airborne radio-echo sounding (RES) surveys are widely used to measure ice thickness in Antarctica. Although minor differences exist between the radar systems that have been employed in Antarctica, they share a common basic premise. An electronic signal is converted to radio waves, which are emitted from an antennae array mounted on the survey platform (e.g. aircraft). This radar pulse propagates through the air and ice sheet, and energy is reflected at interfaces with strong acoustic impedance contrasts (Fig. 1). The strongest reflections are from the air-ice and ice-bed interfaces; weaker reflections are also seen from internal layers within the ice. Upon their return to the carrier platform, the echoes are detected by a receiver and converted back to an electronic signal. The system then records the time delay between the pulse being emitted and received – the two-way travel time.

The ice surface and bed reflectors are extracted ('picked') from each radar trace (Fig. 1). The difference in the two-way travel times of these two reflectors gives the two-way travel time of the radar in the ice, which is multiplied by an assumed radar velocity in ice (*c.* 168 m  $\mu\text{s}^{-1}$ ), with an additional small correction commonly made for the firn layer (the thin layer of snow and uncompacted ice at the top of the ice sheet, which does not generate strong radar reflections) to give the ice thickness. The difference between the ice surface elevation (which can be determined via laser altimetry) and the ice thickness gives the bed elevation. Location and altitude of the radar platform are determined using a global positioning system (GPS).

Up to 2013, *c.* 25 million ice thickness measurements (Fig. 1) had been acquired and incorporated into the Bedmap2 digital

elevation model (DEM) of Antarctica's bedrock topography (Fig. 2) (Fretwell *et al.* 2013). However, approximately only one third of cells within Bedmap2 contain at least one real ice thickness measurement (the grid is at 5 km horizontal resolution), and some areas are >200 km away from the nearest real data point (Fretwell *et al.* 2013). Several multi-season field campaigns have commenced since the publication of Bedmap2, with the aim of filling some of these major data gaps (Fig. 1). This increased data coverage is reflected in the recently developed BedMachineAntarctica DEM (Morlighem *et al.* 2020).

### *Bed topography and ice sheet behaviour*

Antarctica's subglacial topography is important to our understanding of AIS history. It has become increasingly recognized that subglacial topography exerts a fundamental influence on the dynamics of the overlying ice sheet (Wilson *et al.* 2013; Austermann *et al.* 2015; Gasson *et al.* 2015; Colleoni *et al.* 2018), and is therefore an important boundary condition in numerical ice sheet models. Ice sheet models aim to simulate the present dynamics of the AIS and predict the response of the ice sheet to future projected climatic change and, in turn, evaluate likely changes in global sea-levels (Mengel and Levermann 2014; Golledge *et al.* 2015; DeConto and Pollard 2016; Edwards *et al.* 2019). Since bed topography exerts a strong influence on ice sheet dynamics, it is important for any ice sheet model to incorporate an accurate DEM of present-day subglacial topography.

Of particular significance are 'marine ice sheets', which are grounded on bed situated below sea-level. Marine ice sheets that are grounded on an inland-dipping ('reverse sloping') bed are hypothesized to be particularly susceptible to perturbations in atmosphere and ocean temperatures (Mercer 1978; Thomas 1979). In this scenario, when the grounding line of the marine ice sheet retreats, it retreats into deeper water, leading to increased flotation, basal melting and ice discharge, resulting in further retreat and a self-sustained positive feedback (Schoof 2007). This process is known as marine ice sheet instability, and permits a highly non-linear response of the grounding line to initial climate and ocean forcing, creating the possibility of rapid retreat or even catastrophic collapse of marine-based ice sheets (Mercer 1978; Thomas 1979; Scherer *et al.* 1998; Schoof 2007; Joughin and Alley 2011). Ice sheet modelling studies incorporating marine ice sheet instability

From: Martin, A. P. and van der Wal, W. (eds) *The Geochemistry and Geophysics of the Antarctic Mantle*.

Geological Society, London, Memoirs, 56,

<https://doi.org/10.1144/M56-2020-7>

© 2021 The Author(s). This is an Open Access article distributed under the terms of the Creative Commons Attribution License (<http://creativecommons.org/licenses/by/4.0/>). Published by The Geological Society of London. Publishing disclaimer: [www.geolsoc.org.uk/pub\\_ethics](http://www.geolsoc.org.uk/pub_ethics)

G. J. G. Paxman

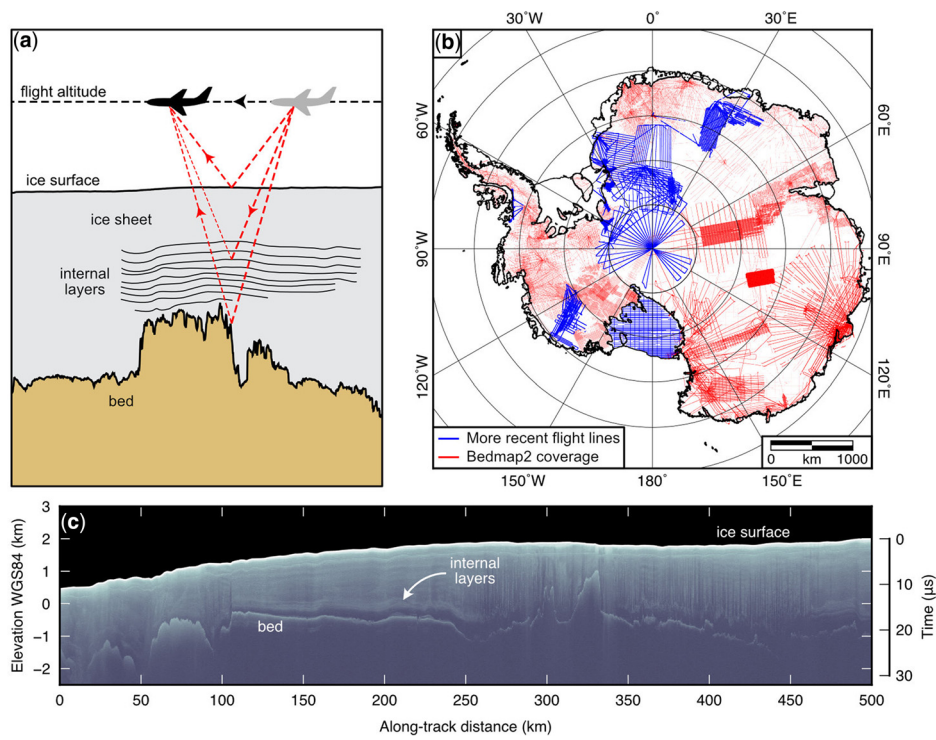


**Fig. 1.** Measurement of ice thickness and subglacial topography using radio-echo sounding (RES). **(a)** Schematic of an airborne RES survey. The aircraft emits a series of radar pulses (red dashed lines), which are reflected at interfaces including the ice surface, internal layers within the ice sheet, and the ice–bed interface. The amount of radar energy reflected depends on the acoustic impedance contrast at the interface. The aircraft then receives the return echoes, and their travel time is used to calculate the depth to the reflector. **(b)** Coverage of RES measurements in Antarctica. Red lines denote surveys that were included in the Bedmap2 compilation (Fretwell *et al.* 2013); blue lines denote more recently acquired survey data (Forsberg *et al.* 2018; Humbert *et al.* 2018; Jordan *et al.* 2018; Karlsson *et al.* 2018; Tinto *et al.* 2019). **(c)** Example of a radar trace (echogram) from Antarctica (Leuschen *et al.* 2016). Elevations are relative to the WGS84 ellipsoid. The y-axis is converted from time to depth assuming a radar velocity in ice of 168 m/ $\mu$ s. Reflectors from the ice surface and ice sheet bed are clearly visible, as are faint internal layer reflections within the ice sheet.

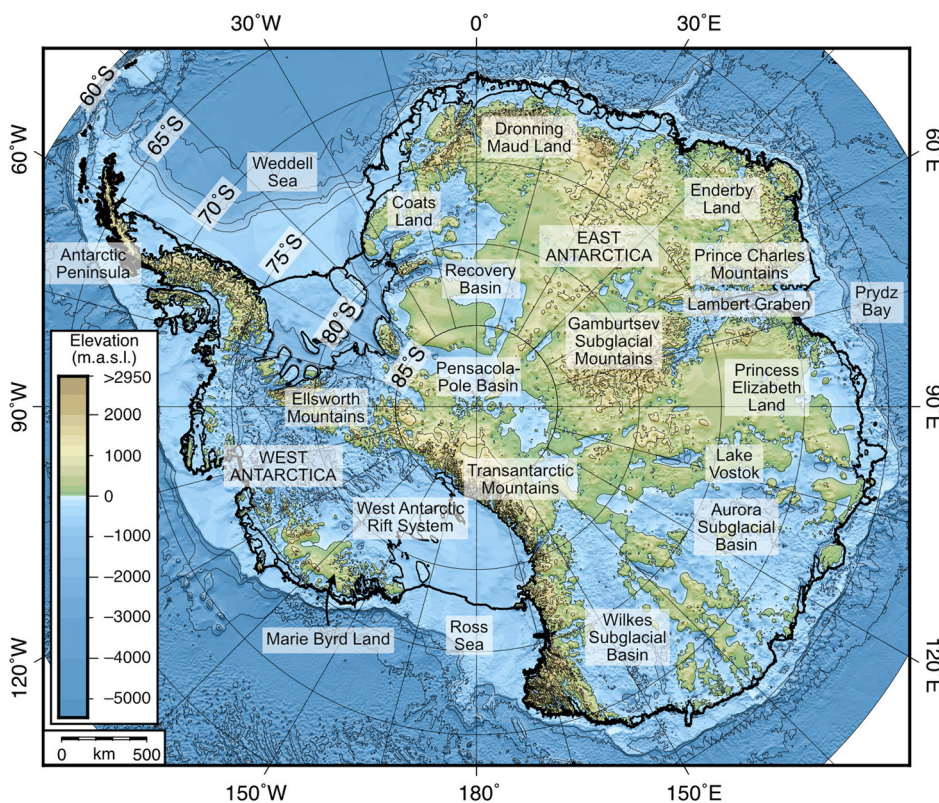


**Fig. 2.** Bed topography of Antarctica. Bed elevations and bathymetry are from the Bedmap2 dataset (Fretwell *et al.* 2013). Elevations are in metres above mean sea-level (m.a.s.l.) and contoured at 1000 m intervals. Major geographical and topographical features are labelled. The dark lines around the edge of the continent denote the modern grounding line and ice shelf calving front. Approximately 45% of the bed is presently situated below sea-level, including the extensive Recovery, Wilkes and Aurora subglacial basins in East Antarctica, wherein the deepest regions are *c.* 2 km below sea-level (Fretwell *et al.* 2013).

## Antarctic palaeotopography

processes (Pollard *et al.* 2015) have predicted global sea-level rise of *c.* 1 m by the end of the current century (DeConto and Pollard 2016). However, probabilistic model projections indicate that these values may significantly overestimate the rate of ice mass loss and sea-level rise (Edwards *et al.* 2019). Moreover, a number of processes have been documented that may counteract marine ice sheet instability, such as slow ice shelf removal rates (Clerc *et al.* 2019), local isostatic uplift of the bed beneath the grounding line (Barletta *et al.* 2018; Kingslake *et al.* 2018), and deformation-induced relative sea-level change (Gomez *et al.* 2010).

Marine-based ice in Antarctica has the potential to contribute *c.* 23 m of global sea-level rise (Fretwell *et al.* 2013); the amount of warming required to induce significant retreat of marine-based parts of the ice sheet, and the likely rate and magnitude of the retreat, are therefore questions of crucial societal importance. In order to constrain these unknowns, attention has focused on records of AIS stability during past warm periods in Earth's history that may serve as analogues for future climate conditions. Ice sheet models are typically assessed by how well they can reproduce past ice sheet behaviour (as constrained from geological and sea-level records) before they can be confidently used to predict the response of the AIS to projected future climate scenarios. Since certain areas of the subglacial topography of Antarctica have been extensively modified since glacial inception *c.* 34 million years ago (Jamieson *et al.* 2010; Wilson *et al.* 2012; Paxman *et al.* 2019b; Pollard and DeConto 2019), it is unrealistic to use the modern bed topography when attempting to model early Antarctic ice sheets. Using a more realistic reconstruction of subglacial topography for past time intervals has the potential to increase the robustness of ice sheet model results and, in turn, (a) facilitate improved understanding of the response of past Antarctic ice sheets to climatic change (DeConto and Pollard 2003a; Wilson *et al.* 2013) and (b) engender greater confidence in projections of future ice sheet stability, mass loss and sea-level change.

Additionally, the morphology of subglacial topography is an important repository of information pertaining to past ice sheet

dynamics. A landscape contains a record of the processes that have acted to shape it, and Antarctic geomorphology studies typically aim use age relationships and the morphology of landscape features to determine the history of the landscape and the processes that produced it. This analysis can reveal insights as to the spatial extent, dynamics and behaviour of past ice sheets, in particular during past warmer climate intervals potentially analogous to the future. For example, RES data have revealed subglacial landforms and areas of enhanced glacial erosion within the Aurora Subglacial Basin in East Antarctica, several hundred kilometres inland of the modern ice margin (Young *et al.* 2011; Aitken *et al.* 2016). Such landforms likely formed near the margin of a dynamic early ice sheet with a more restricted extent than at the present-day.

## Antarctic glacial history

The timescales over which changes in Antarctic bed topography are most significant in this context are intrinsically linked to the intervals during which ice sheets have been present in the Southern Hemisphere. Marine oxygen isotope records indicate that the Earth has been experiencing a long-term cooling trend since the Early Eocene Climatic Optimum (*c.* 51 Ma; Fig. 3) (Zachos *et al.* 2001). The first appearance of continental-scale ice sheets in Antarctica is widely agreed to have occurred around the time of the Eocene–Oligocene boundary (*c.* 34 Ma) (Zachos *et al.* 2001; Coxall *et al.* 2005; Liu *et al.* 2009), which marks the transition between the 'greenhouse world' of the Cretaceous–Eocene and the 'icehouse world' that Earth has inhabited since the start of the Oligocene (Fig. 3). Stratigraphic records indicate that ice sheet growth occurred in a stepwise fashion across the Eocene–Oligocene transition, in concert with the marine oxygen isotope record (Coxall *et al.* 2005; Katz *et al.* 2008; Scher *et al.* 2011; Passchier *et al.* 2017). However, it is important to note that although this climate transition marks the first appearance of large-scale Southern Hemisphere ice sheets,

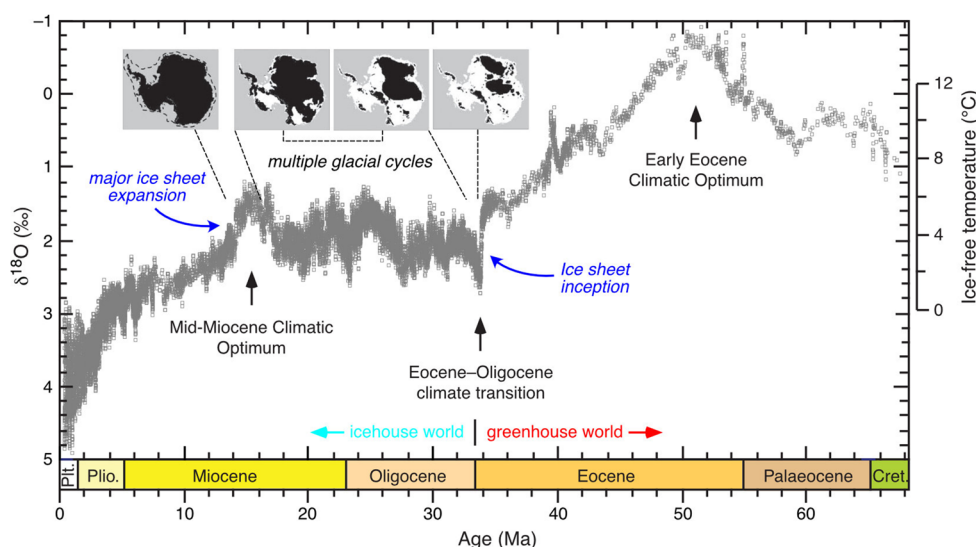


**Fig. 3.** Cenozoic ice sheet and climate history of Antarctica (modified from Zachos *et al.* 2008). Curve shows the Cenozoic stacked benthic foraminifera oxygen isotope record, based on deep-sea sediments obtained at Deep Sea Drilling Project and Ocean Drilling Program sites (Zachos *et al.* 2001, 2008). The raw data have been smoothed using a five-point running mean.  $\delta^{18}\text{O}$  isotope values are given in parts per thousand (‰). The temperature scale is calculated for ice-free conditions, so only applies to the time interval preceding glaciation in Antarctica. The greenhouse-icehouse transition and the formation of large-scale ice sheets on Antarctica coincides with the step increase in  $\delta^{18}\text{O}$  at the Eocene–Oligocene boundary (*c.* 34 Ma). The approximate ice extents for different stages (shaded black) are derived from ice sheet modelling (Jamieson *et al.* 2010). The Oligocene to middle Miocene witnessed numerous glacial cycles, with the ice sheet waxing and waning in concert with orbital cycles. Subsequent Miocene cooling allowed the ice sheet to advance to the continental shelf edge, perhaps on multiple occasions. Abbreviations: Cret. = Cretaceous; Plio. = Pliocene; Plt. = Pleistocene.

ephemeral ice sheets and/or mountain glaciers may have existed on Antarctica at an earlier stage (Carter *et al.* 2017).

The mechanisms behind the precise timing of glacial inception in Antarctica remain subject to continuing debate. However, it is widely believed that continental-scale glaciation on Antarctica was triggered by a drop in atmospheric pCO<sub>2</sub> levels below a threshold (DeConto and Pollard 2003a; DeConto *et al.* 2008; Pearson *et al.* 2009; Pagani *et al.* 2011) combined with associated internal feedbacks within the carbon cycle (Tripathi *et al.* 2005; Zachos and Kump 2005; Reusch 2011; Scher *et al.* 2011). The opening/deepening of ocean gateways around Antarctica, in particular the Drake Passage and the Tasman Gateway, may have also played a role in the timing of glaciation (Kennett 1977; DeConto and Pollard 2003b).

Cyclicity in marine oxygen isotope and sedimentary records from drill cores around the Antarctic margin indicates that the early Antarctic ice sheets waxed and waned in concert with orbital cycles during the Oligocene and early Miocene (Hambrey *et al.* 1991; Zachos *et al.* 1997, 2001; Naish *et al.* 2001; Barrett 2008). Approximately 33 glacial cycles have been detected in this interval, and the sedimentary record suggests that meltwater was abundant, with conditions similar to present-day Greenland (Naish *et al.* 2001; Sugden and Jamieson 2018). Marine sediment cores from the Ross Sea revealed an erosional hiatus at the Oligocene–Miocene boundary (*c.* 23 Ma) indicative of a major episode of global cooling and ice sheet expansion (Naish *et al.* 2001), which has also been inferred from a contemporaneous benthic foraminiferal oxygen isotope shift that implies a significant increase in ice volume (Fig. 3) (Zachos *et al.* 2001). Following the mid-Miocene Climatic Optimum, a gradual cooling trend commenced at *c.* 14 Ma (Fig. 3). Decreasing air and ocean temperatures allowed the AIS to expand significantly under an arid polar climate (Zachos *et al.* 2001), and the oscillatory and more restricted ice masses evolved into a major and persistent continental ice sheet (Fig. 3) (DeConto and Pollard 2003a; Jamieson *et al.* 2010). The ice sheet extended to the continental shelf edge, perhaps on multiple occasions, before retreating and stabilizing with dimensions similar to that of the present-day (Sugden and Denton 2004).

This multi-faceted glacial history over the past 34 million years provides a large window of time for significant topographic and landscape evolution to occur in Antarctica. Efforts to understand palaeotopography in Antarctica have

therefore primarily focused on the time period from glacial inception at *c.* 34 Ma to the present day (Jamieson and Sugden 2008; Wilson and Luyendyk 2009; Wilson *et al.* 2012; Paxman *et al.* 2019b). However, attempts are also ongoing to produce reconstructions of Antarctic palaeotopography during the early Cenozoic and Late Cretaceous, which will be important boundary conditions for the modelling of older ice masses, regional ocean and atmosphere circulation, and palaeoclimate.

#### Framework of landscape evolution in Antarctica

Landscape evolution reflects the competition between ‘solid Earth’ processes such as tectonics, which act to increase or decrease the elevation of the crust, and ‘Earth surface’ processes such as erosion and sedimentation, which modify it. In Antarctica, the mantle facilitates the generation of surface topography via:

1. The flexural isostatic response to load redistribution (via e.g. erosion, sedimentation, movement on faults), which is governed by the balance of forces in the crust and mantle lithosphere and causes uplift or subsidence of the Earth’s surface.
2. Heating or cooling of the lithosphere, which alters the density of the crust/mantle lithosphere and drives a transient phase of surface uplift or subsidence. Heating can also induce volcanic activity, causing emplacement of magmatic material on the Earth’s surface or intrusion of magmatic material within the crust.
3. Viscous normal tractions applied to the base of the lithosphere by density-driven convective flow within the mantle (‘dynamic topography’).

Each of these processes (Fig. 4) is to a greater or lesser extent influenced by the properties of the mantle; each is described in turn in the following sections of this chapter.

#### Isostasy

##### Elastic plate flexure

Isostatic adjustment occurs in response to the redistribution of loads on the surface of, or within, the lithosphere on

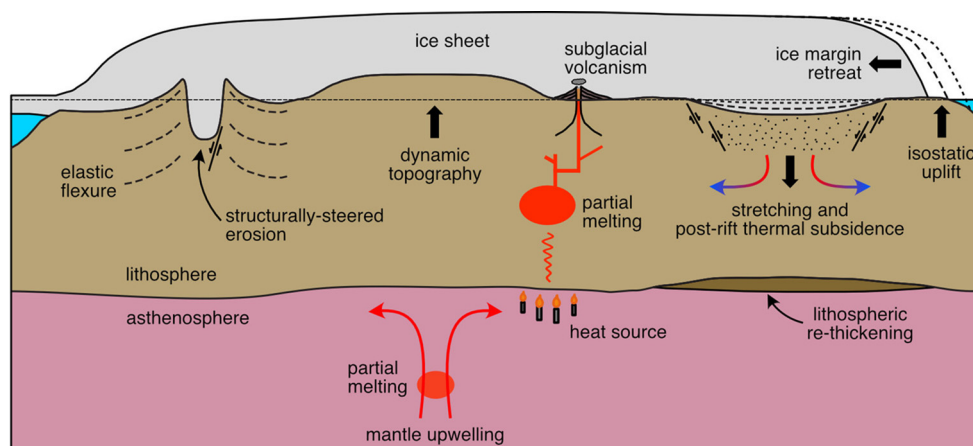


**Fig. 4.** Schematic summary of the interactions between mantle processes and topography beneath ice sheets. Changes in surface loading due to (e.g.) erosion or ice margin retreat induce a flexural isostatic response within the elastic lithosphere. Topographic subsidence occurs in response to lithospheric stretching and subsequent ‘post-rift’ cooling, re-thickening and densification, and commonly allows sediments to accumulate in the resulting basin. Deposition of sediments in turn triggers a flexural isostatic response, causing further subsidence. Heating of the lithosphere can induce partial melting, which leads to subglacial volcanism. Heating can also induce topographic uplift, as can normal tractions imparted on the base of the lithosphere by the convecting viscous mantle (dynamic topography).

wavelengths of order 100–1000 km. Landscape evolution processes involve the redistribution of surface and sub-surface material on these length scales, and therefore induce vertical surface displacement via the isostatic re-equilibration of the lithosphere. Moreover, isostasy is the process by which many solid Earth phenomena cause changes in surface topography, and is therefore the most ubiquitous link between mantle properties and landscape evolution processes (Fig. 4).

The flexural isostatic model states that surface and sub-surface loads are supported by a combination of (a) buoyancy forces imparted on the base of the crust by the mantle lithosphere, which arise due to the difference in density between crust and mantle (Airy isostasy), and (b) elastic bending forces within the lithosphere. The ratio of buoyancy forces and elastic bending forces is a function of the wavelength of the load and also the flexural rigidity of the lithosphere. The flexural response of the lithosphere to (un)loading over geological timescales ( $>10^6$  years) may be computed by modelling the lithosphere as a thin elastic plate overlying an inviscid (non-viscous) substrate (the asthenospheric mantle) (Watts 2001; Watts *et al.* 2013). The general two-dimensional flexure equation giving the downward deflection ( $w$ ) of the elastic plate in response to loading ( $h$ ) is given by

$$\nabla^2[D(x, y)\nabla^2w(x, y)] + (\rho_{\text{mantle}} - \rho_{\text{infill}})gw(x, y) = (\rho_{\text{load}} - \rho_{\text{displace}})gh(x, y) \quad (1)$$

where

$$D(x, y) = \frac{ET_e(x, y)^3}{12(1 - \nu^2)} \quad (2)$$

is the flexural rigidity of the lithosphere as a function of spatial dimensions  $x$  and  $y$ .  $E$  (Young's modulus; 100 GPa) and  $\nu$  (Poisson's ratio; 0.25) are elastic constants and the density terms ( $\rho$ ) depend on the particular loading or unloading scenario being considered. The densities of the load and the mantle are given by  $\rho_{\text{load}}$  and  $\rho_{\text{mantle}}$  respectively. The terms for  $\rho_{\text{displace}}$  and  $\rho_{\text{infill}}$  can be ignored for subaerial surface loads, but for subaqueous loads the density contrasts between (i) the load and the displaced water, and (ii) the mantle and the material filling in the flexural moat (e.g. water, sediment) must also be included.

The spatial pattern (amplitude and wavelength) of the flexural isostatic response to (un)loading is determined by the flexural rigidity ( $D$ ) or its proxy, the effective elastic thickness ( $T_e$ ) of the lithosphere (Watts 2001).  $T_e$  is a measure of the equivalent thickness the lithosphere would have if it behaved as a perfectly elastic plate overlying an inviscid fluid asthenospheric mantle, as is assumed by the thin elastic plate model (equation 2). In reality, the composition and rheology of the lithosphere is strongly heterogeneous, so  $T_e$  is more appropriately conceptualized as a proxy for the depth-integrated strength of the lithosphere (Watts and Burow 2003). An important implication of the flexure model is that provided the lithosphere has a finite rigidity/strength, vertical surface displacement occurs beyond the spatial limits of the (un)load (Fig. 4); flexural isostasy is therefore known as 'regional isostasy'.

### Flexural rigidity of the Antarctic lithosphere

Flexurally rigid lithosphere is associated with long-wavelength, low-amplitude flexural displacement, whereas flexurally weak lithosphere is associated with short-wavelength, high-amplitude flexural displacement. Since the effective elastic thickness governs the pattern of flexural adjustment to load redistribution, the depth-integrated strength of the Antarctic

lithospheric mantle is an important parameter in landscape evolution models. Attempts to estimate  $T_e$  in Antarctica can be divided into two broad categories.

1. Forward modelling techniques, whereby an observed manifestation of flexure such as a deflected/warped topographic surface and/or its associated gravity anomaly is compared to the predictions of an elastic plate model in which  $T_e$  can be adjusted. The value of  $T_e$  in the model that yields the best fit with the observed flexure is regarded as the estimate of  $T_e$  at the time of loading for the region under consideration. Such methods have recovered  $T_e$  values of  $5 \pm 5$  km for parts of the West Antarctic Rift System (Jordan *et al.* 2010; Wenman *et al.* 2020),  $c. 5$  km close to the front of the Transantarctic Mountains, increasing to  $c. 85$ – $115$  km beneath the Wilkes Subglacial Basin (Stern and ten Brink 1989; ten Brink *et al.* 1997; Stern *et al.* 2005), and  $20$ – $25$  km in the Recovery Basin (Paxman *et al.* 2017) (Fig. 5a).
2. Inverse (spectral) modelling of observed gravity anomalies and subglacial topography. The two spectral parameters commonly used to estimate  $T_e$  from gravity and topography data are the free-air admittance and the Bouguer coherence. The free-air admittance is the linear transfer function between the free-air anomaly and the topography in the frequency domain, while the Bouguer coherence is essentially the square of the Pearson product-moment correlation coefficient between the Bouguer gravity anomaly and the topography, again computed in the frequency domain (Kirby 2014). The forms of these two spectral parameters as a function of wavelength can be used to estimate  $T_e$ , and have recovered values of  $c. 35$  km in the Weddell Sea embayment (Studinger and Miller 1999),  $c. 10$  km in the Gamburtsev Subglacial Mountains (Paxman *et al.* 2016) and  $c. 20$  km in the Recovery Basin (Paxman *et al.* 2017) (Fig. 5b).

While the forward modelling methods are robust where a clear surface manifestation of flexure, such as tilted palaeoland surfaces, can be discerned (ten Brink *et al.* 1997; Paxman *et al.* 2017), reference surfaces with a known geometry prior to flexural warping are rarely identified in Antarctica given the lack of surface exposure. In addition, forward models recover the  $T_e$  pertaining to the time at which loading occurred, which is not necessarily equivalent to the contemporary  $T_e$ . The ability of  $T_e$  to evolve over geological timescales (e.g. Watts *et al.* 2013), has been documented for the rifted basins in the Ross Sea (Karner *et al.* 2005). The potential temporal variation of  $T_e$  adds an additional level of uncertainty in reconstructing flexure in Antarctica over long timescales.

By contrast, the inverse spectral methods can be applied over large areas, since most of Antarctica has fairly well-established topography (Fretwell *et al.* 2013) and gravity anomaly (Scheinert *et al.* 2016) grids. However, the validity of the results derived from the spectral methods, particularly the Bouguer coherence, has been questioned where there is a lack of clear coherence between the topography and the gravity anomaly, which may be caused by the presence of buried loads (i.e. loads with no surface topographic manifestation) or the modification of topography by erosion (McKenzie and Fairhead 1997; Watts 2001; Kirby 2014). It has been argued that the  $T_e$  estimates derived from the Bouguer coherence maybe consequently be biased towards high values and should be considered upper bounds rather than best estimates (McKenzie and Fairhead 1997). Moreover, in places of low RES coverage, Antarctic bed topography is often determined by inversion of gravity anomalies, which introduces circularity when  $T_e$  is estimated from the relationship between topography and gravity anomalies. These

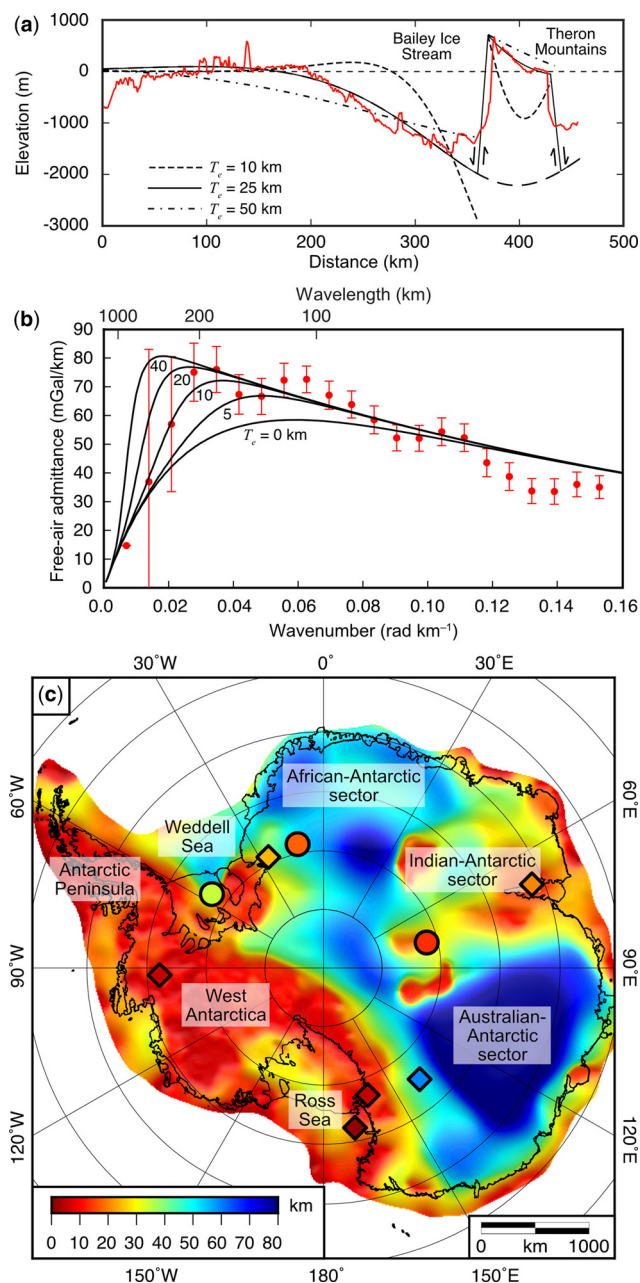


**Fig. 5.** Effective elastic thickness estimation in Antarctica. (a) Forward modelling of flexed topography along a profile crossing the Bailey Ice Stream and Theron Mountains, East Antarctica (modified from Paxman *et al.* 2017). Elastic plate models (black lines) indicate that the observed topography (red line) is best fit with a  $T_e$  value of 25 km. (b) Inverse (spectral) modelling of topography and gravity anomaly data for the region of East Antarctica including the profile in panel a. Comparison of the calculated free-air admittance (red circles with standard error bars) with model curves recovers a best fitting  $T_e$  of 18 km (modified from Paxman *et al.* 2017). (c)  $T_e$  map for Antarctica derived using a fan wavelet method to compute the Bouguer coherence (Chen *et al.* 2018). Coloured shapes denote published regional  $T_e$  estimates using forward (diamonds) and inverse (circles) modelling.

limitations mean that there is considerable uncertainty surrounding the use of inverse spectral methods to estimate  $T_e$  in Antarctica.

Fan wavelet techniques have recently been employed to determine variations in  $T_e$  across the entirety of Antarctica using the admittance and coherence methods (Ji *et al.* 2017; Chen *et al.* 2018). These methods show a strong contrast between predominantly high values in East Antarctica ( $T_e$

~60–80 km) and low values in West Antarctica ( $T_e$  ~5–20 km) (Chen *et al.* 2018). However, the fan wavelet techniques also recover considerable variability within East Antarctica, with particularly high  $T_e$  values found in the Australian–Antarctic and Africa–Antarctic sectors, but relatively low values found in the Indian–Antarctic sector, including the Lambert Graben and Gamburtsev Subglacial Mountains (Fig. 5c) (Chen *et al.* 2018).

Spatial patterns in Antarctic  $T_e$  recovered by both forward and inverse models tend to show broad first-order agreement, albeit from a limited set of results (Fig. 5c). Significant uncertainty persists, however, as to the absolute values of  $T_e$ . The finding of a relatively weak West Antarctic lithosphere and a relatively rigid East Antarctic lithosphere may reflect the first-order differences between physical properties such as topography, crustal thickness, lithosphere thickness, lithosphere age, upper mantle viscosity, and heat flux in West and East Antarctica (An *et al.* 2015a, b). The differences in  $T_e$  within East Antarctica are indicative of spatial heterogeneities in the East Antarctic lithosphere, which may arise from the distinct tectonic histories of the different provinces (Chen *et al.* 2018). However, despite its importance in the context of long-term tectonic and topographic evolution,  $T_e$  in Antarctica remains poorly constrained.

### Flexure and palaeotopography

**Ice sheet loading.** The most visible surface load in Antarctica today is the ice sheet itself (Fig. 6). Isostatic models indicate that complete removal of the modern ice sheet load would result in up to 1 km of bedrock uplift, and an average increase in bedrock elevation of *c.* 600 m (Paxman *et al.* 2019b). Any palaeotopography prior to Antarctic glaciation, or during a time at which the ice sheet was more restricted than today, was most likely characterized by higher average elevations. Under the modern ice sheet, *c.* 45% of the bed currently situated beneath grounded ice is situated below sea-level, whereas complete deglaciation would reduce this to *c.* 19% (Paxman *et al.* 2019b). Ice sheet loading therefore has a significant effect on the extent of marine-based ice, which is most vulnerable to potential rapid retreat (see section 1.2). For an in-depth review of glacial isostatic adjustment on decadal to multi-millennial timescales, see Nield and Barletta (this volume).

**Erosional unloading.** Parts of the subglacial landscape of Antarctica have also been significantly modified by glacial erosion (Taylor *et al.* 2004; Jamieson *et al.* 2005). Removal of crustal mass by erosion (‘erosional unloading’) induces an isostatic response from the lithosphere, causing uplift of the remaining topography (Fig. 6) (Molnar and England 1990). Selective linear erosion, whereby basal melting and erosion are concentrated beneath thick ice in glacial troughs, while neighbouring peaks remain preserved beneath non-erosive ice (Sugden and John 1976) and uplifted by the regional flexural adjustment to erosional unloading, is therefore optimal for creating substantial topographic relief.

Incision beneath major outlet glaciers dissecting mountain ranges around the Antarctic margin, such as the Beardmore and Byrd Glaciers in the Transantarctic Mountains (TAM) and the Recovery and Slessor Glaciers bounding the Shackleton Range, has produced subglacial troughs situated up to 3 km below sea-level and differences in elevation between mountain peaks and trough floors of up to *c.* 5 km over lateral distances of as little as 50 km (Fretwell *et al.* 2013; Morlighem *et al.* 2020). Elastic plate models show that the isostatic response to glacial incision can account for up to 2000 m of peak uplift in the central TAM and 1000 m in the Shackleton Range, which represents up to *c.* 50% of the total peak

## Antarctic palaeotopography

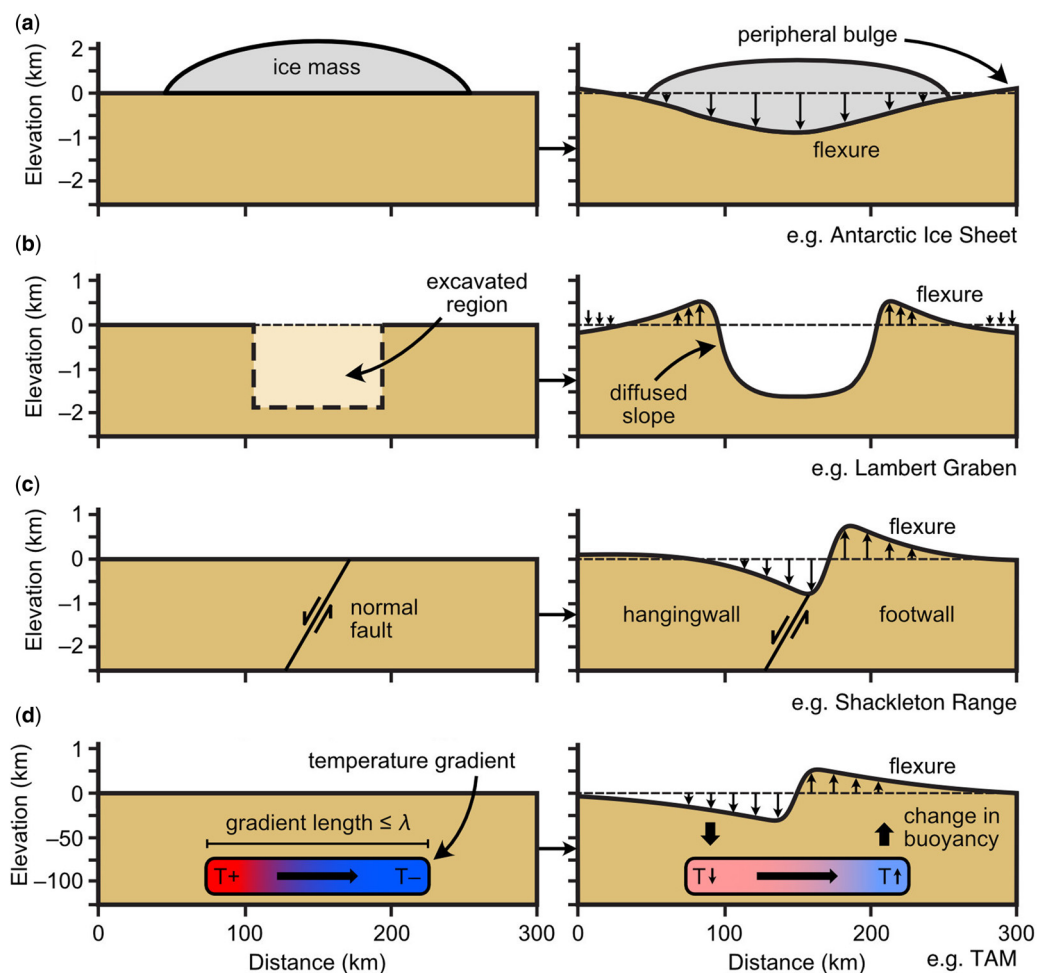


**Fig. 6.** Causes of lithospheric flexure in Antarctica. Diagrams are schematic, although representative horizontal and vertical scales are provided. (a) Ice loading, causing the land to be depressed beneath an ice mass, such as the AIS. Peripheral bulges are uplifted around the margin of the ice sheet. (b) Erosional unloading, caused by excavation of material by rivers or glaciers. The flexed topography exhibits uplifted flanks dipping gently away from the valley. Such topography is observed around numerous large outlet glaciers in Antarctica, such as the Lambert Glacier (White 2013). (c) Mechanical unloading, caused by shear along a normal fault plane. The footwall block is unloaded and flexurally uplifted, whereas in the hangingwall block surface material is replaced by mantle, causing loading and flexural subsidence (Weissel and Kerner 1989). Such topography is observed along the flanks of major extensional fault systems, such as in the Shackleton Range (Paxman *et al.* 2017). (d) Thermal expansion (/ ‘unloading’), caused by horizontal heat conduction within the lithosphere. Heat is conducted from areas of high temperature to areas of low temperature, and modifies the thermal buoyancy of the lithosphere, which induces a flexural response if the length of the thermal gradient  $\leq$  the flexural wavelength of the lithosphere ( $\lambda$ ). This process has been hypothesized to partially explain the uplift of the Transantarctic Mountains (TAM) (Stern and ten Brink 1989; ten Brink *et al.* 1997; Brenn *et al.* 2017).

elevations of the mountains (Stern *et al.* 2005; Paxman *et al.* 2017). In addition, flexural models, alongside geological observations such as uplifted fjordal sediments and detrital thermochronology, indicate that *c.* 3 km of incision within the Lambert Graben (Tochilin *et al.* 2012; Thomson *et al.* 2013; White 2013) has driven up to 1.4 km of post-Eocene flexural uplift along the graben flanks (Paxman *et al.* 2019b). In each of these examples, the high-amplitude flexural response is partly facilitated by relatively low regional  $T_c$  values (Fig. 5) and has helped to generate as much as 4 km of additional topographic relief.

Many outlet glaciers across Antarctica appear to follow the underlying tectonic structure, such as the Lambert Glacier above the Mesozoic Lambert Graben (Ferraccioli *et al.* 2011). Pre-existing fault systems and associated topographic relief were likely first exploited by pre-glacial river systems (Jamieson *et al.* 2014; Sugden and Jamieson 2018) and, in turn, by the early ice sheets, which progressively excavated the valleys to form deep subglacial troughs. Topographic steering became increasingly effective and ice flow and subglacial erosion became strongly focused within the troughs, whereas removal of mass by erosion caused the adjacent

highlands to be flexurally uplifted to elevations where relatively thin, non-erosive ice predominates, preserving the mountain peaks (Kessler *et al.* 2008; Paxman *et al.* 2017). Significant topographic relief can therefore be generated in Antarctica through a combination of (a) the relative efficacy of glacial erosion (Koppes and Montgomery 2009), (b) peak preservation beneath non-erosive ice, and (c) flexural uplift induced by a relatively weak mantle lithosphere. Isostasy and lithospheric flexure can therefore drive and amplify feedbacks between tectonic structure, topography, climate and ice sheet behaviour.

Prior to glacial erosion and associated flexural uplift, the palaeotopography of Antarctica would have been characterized by considerably lower topographic relief, especially in the vicinity of the deep subglacial troughs near the coast, where fluvial valley networks could have only incised down to base level (Wilson *et al.* 2012; Thomson *et al.* 2013; Maritati *et al.* 2016; Paxman *et al.* 2017). The proportion of Antarctic topography situated below sea-level *c.* 34 Ma has been estimated at *c.* 6%, compared to *c.* 19% today (under ice-free conditions), with considerably less ice situated on deep, reverse-sloping beds (Paxman *et al.*

2019b). The overall effect of this change would be that earlier ice sheets were comparatively less susceptible to rapid, irreversible retreat associated with marine ice sheet instability processes. Prior to flexural uplift, the elevated terrain around the Antarctic margins would have been situated at lower average elevations at *c.* 34 Ma, which could have influenced the timing and scale of early ice sheet nucleation. By contrast, the central highlands of East Antarctica, where long-term erosion rates are low (Jamieson and Sugden 2008; Cox *et al.* 2010; Jamieson *et al.* 2010; Rose *et al.* 2013), and flexural responses to fluvial and alpine-style erosion are comparatively small (Paxman *et al.* 2016), have most likely remained relatively topographically stable over most of the past 34 myr.

*Mechanical unloading and thermal expansion.* Lithospheric flexure can also occur in response to mechanical unloading and thermal expansion. Mechanical unloading takes place in extensional settings (e.g. rift systems) when slip on a normal fault causes unloading of the footwall block by removal of the hanging wall; the result is flexural isostatic rebound and uplift of the footwall rift flank (Fig. 6) (Weissel and Karner 1989). Thermal expansion (sometimes termed ‘thermal unloading’) occurs when the density of the lithosphere is reduced owing to lateral/vertical conduction of heat, which can induce a flexural response if the length of the thermal gradient does not exceed the flexural wavelength of the lithosphere (Fig. 6). The TAM have been modelled as a flexurally-uplifted flank of the West Antarctic Rift System (WARS) arising from mechanical unloading on range-parallel normal faults bounding the WARS and thermal expansion due to lateral conduction of heat from higher-temperature mantle lithosphere beneath the WARS (see the ‘West Antarctic Rift System’ section) to lower-temperature mantle lithosphere beneath East Antarctica (Stern and ten Brink 1989; ten Brink *et al.* 1997; Lawrence *et al.* 2006).

However, the TAM chain exhibits considerable variation in elevation and width along its length, which cannot be easily explained by uniform flexure along the mountain front (Olivetti *et al.* 2018; Paxman *et al.* 2019a). This variation may in part be explained by the presence of heterogeneous thermal anomalies within the upper mantle beneath the TAM front, which may provide spatially variable buoyant thermal loads (Lawrence *et al.* 2006; Brenn *et al.* 2017). Particularly problematic however are the southern TAM, where a high plateau extends for more than 300 km into East Antarctica (Fretwell *et al.* 2013). It is difficult to envisage how edge-driven flexure at the front of the TAM alone can account for such a broadly distributed, long-wavelength pattern of uplift, even for a highly rigid lithosphere (Paxman *et al.* 2019a) (see also the ‘Transantarctic Mountains’ section).

The significance of the location of the TAM along the tectonic boundary between West and East Antarctica has been noted by a number of authors (ten Brink *et al.* 1997; van Wijk *et al.* 2008; Brenn *et al.* 2017; Ebbing *et al.* 2018). This boundary likely had a bearing, at least in part, on the uplift of the TAM. Numerical models of lithospheric extension indicate that the inherited tectonic boundary between West Antarctica and cratonic East Antarctica focused extensional deformation at the craton edge, resulting in a strongly asymmetrical pattern of TAM uplift (van Wijk *et al.* 2008). Although the mechanism for TAM uplift remains debated (see the ‘Transantarctic Mountains’ section), the presence of an inherited tectonic boundary and the contrasting lithospheric properties of East and West Antarctica have likely played a significant role in the tectonic and topographic evolution of the TAM.

Inherited fault systems may also have played an important role in the topographic uplift of highlands such as the Shackleton Range and Gamburtsev Subglacial Mountains, where modelling studies indicate that mechanical unloading along border faults may have contributed up to 1 km of flexural uplift (Ferraccioli *et al.* 2011; Paxman *et al.* 2017). In the case of the Gamburtsevs, fault activity may be related to rifting within the Mesozoic East Antarctic Rift System (Ferraccioli *et al.* 2011), while fault activity in the Shackleton Range region may have most recently occurred in association with Weddell Sea rifting during the Cretaceous (Krohne *et al.* 2016; Jordan *et al.* 2017).

## Thermal subsidence

Continental extension and rifting are significant drivers of surface topographic subsidence. During the ‘syn-rift’ phase, stretching and faulting are associated with thinning of the crust and lithosphere, which in turn leads to surface subsidence in order to retain isostatic equilibrium. The extent of crustal thinning is quantified by the stretching factor ( $\beta$ ), which is defined as the ratio of original crustal thickness to final crustal thickness. Rifting is also associated with elevated lithospheric heat flux; in the ‘post-rift’ phase, following the cessation of extensional faulting, the decay of the thermal anomaly via heat conduction causes cooling and densification of the lithosphere, which in turn drives subsidence of the Earth’s surface (McKenzie 1978). Since lithospheric cooling is a transient process, thermal subsidence occurs over a protracted period of tens to hundreds of millions of years following a rifting event. It is therefore important to consider the effects of ‘post-rift’ thermal subsidence in the evolution of Antarctic palaeotopography since *c.* 34 Ma.

### West Antarctic Rift System

The West Antarctic Rift System (WARS) is believed to extend from the Ross Sea embayment through West Antarctica to the Bellingshausen Sea (Fig. 7) (LeMasurier *et al.* 1990; LeMasurier and Landis 1996; Winberry and Anandakrishnan 2004; Jordan *et al.* 2010; Bingham *et al.* 2012). The presence of an extensive rift system beneath the West Antarctic Ice Sheet (WAIS) is highly significant, because the low-lying topography (in places as deep as 2.5 km below sea-level (Fig. 7)) is hypothesized to render the WAIS vulnerable to rapid retreat due to marine ice sheet instability processes (Mercer 1978; Thomas 1979; Schoof 2007; Joughin and Alley 2011). Moreover, the bedrock geology and crustal structure of the rift system may influence the on-going and future dynamics of the overlying glaciers (Studinger *et al.* 2001; Rignot *et al.* 2008; Bingham *et al.* 2012), which in turn affect the stability of the wider ice sheet.

Rifting in West Antarctica is thought to have commenced at *c.* 80–100 Ma (Siddoway *et al.* 2004), with the WARS subsequently experiencing 300–600 km of extension during the late Cretaceous and early Cenozoic (Behrendt *et al.* 1991; Cande *et al.* 2000; Wilson and Luyendyk 2009). Consequences of this extension were the separation of Marie Byrd Land from East Antarctica and the opening of the Ross Sea basin (Decsari *et al.* 2007). Relative motion between East and West Antarctica was historically believed to have ended abruptly in the late Oligocene on the basis of marine magnetic anomalies from the northern Ross Sea (Cande *et al.* 2000). However, more recently acquired magnetic anomaly data indicate that motion between East and West Antarctica may have persisted up to the mid-Miocene (Granot and Dyment 2018). Seismic and gravity

## Antarctic palaeotopography

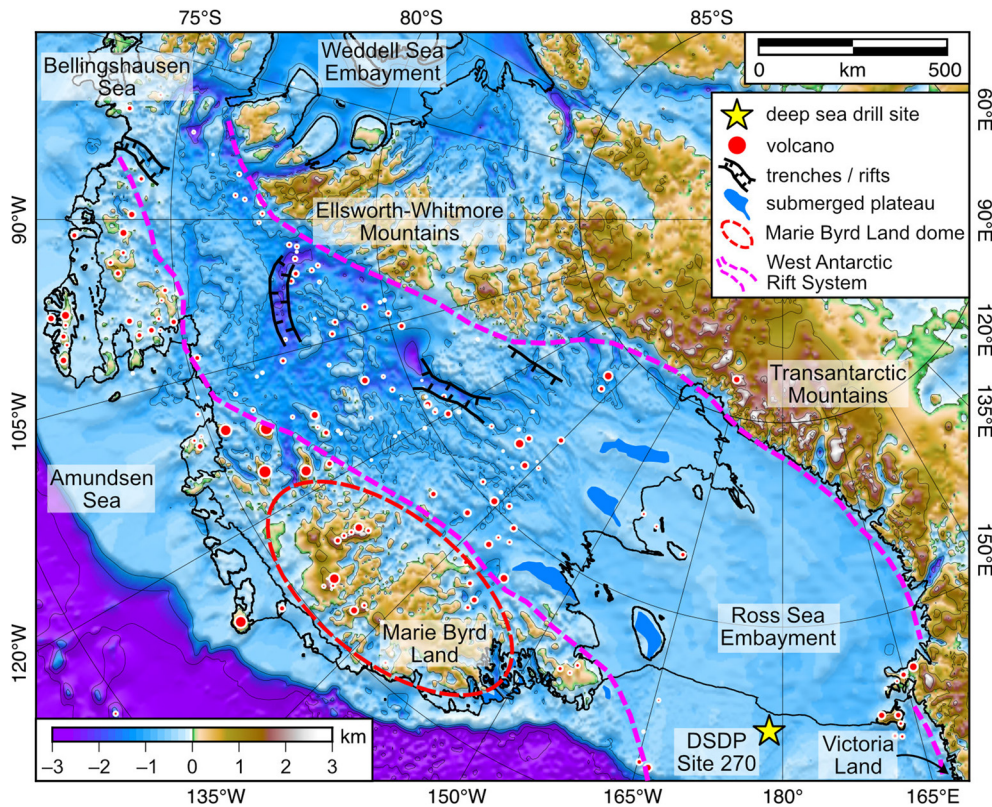


**Fig. 7.** West Antarctic Rift System. Present-day bed elevations are shown relative to mean sea-level (Paxman *et al.* 2019b). Contour interval is 1 km. Dashed magenta lines show the extent of the West Antarctic Rift System. An explanation of the symbology is provided in the figure legend. Red circles denoting volcanic edifices are proportional (4x true scale) to the basal diameter of the cone (van Wyk de Vries *et al.* 2018). Subglacial trenches and rift valleys (black outlines), as well as submerged flat-topped bedrock platforms (blue polygons) are imaged by radar and gravity/magnetic anomaly data (Bell *et al.* 1998; Studinger *et al.* 2001; Wilson and Luyendyk 2006; Bingham *et al.* 2012).

data have recovered crustal thicknesses as low as 21 km beneath the WARS (Winberry and Anandkrishnan 2004; Jordan *et al.* 2010; An *et al.* 2015a), indicating that the region has undergone significant crustal extension and thinning.

Rift-related magmatism appears to have commenced at *c.* 48 Ma in the form of large alkaline plutons exposed in northern Victoria Land (Rocchi *et al.* 2002), where airborne magnetic data suggest similar intrusions may be extensive (Ferraccioli *et al.* 2009). By contrast, Cenozoic intrusive magmatism in Marie Byrd Land began at *c.* 34 Ma (Rocchi *et al.* 2006). Effusive magmatism, in the form of Cenozoic volcanoes, has been documented in Victoria Land, Marie Byrd Land and across the WARS (LeMasurier *et al.* 1990). Dating of edifices and associated deposits indicates that the earliest volcanism commenced at *c.* 30 Ma, and a significant fraction of volcanic deposits date from after the mid-Miocene (*c.* 14 Ma) (Stump *et al.* 1980; LeMasurier *et al.* 1990; LeMasurier and Landis 1996; Rocchi *et al.* 2006; Shen *et al.* 2017). In addition to exposed magmatic rocks, aeromagnetic anomalies indicate that subglacial flood basalts may be preserved within the WARS (Behrendt *et al.* 1994). A recent inventory also indicates that there may be in excess of 138 subglacial volcanic cones across the WARS (van Wyk de Vries *et al.* 2018) (Fig. 7), supporting the presence of an extensive and diffuse alkaline magmatic province (Finn *et al.* 2005).

An implication of the thermotectonic history of the WARS is that the palaeotopography of West Antarctica was considerably higher prior to and during late Cretaceous and Cenozoic crustal extension and heating than at the present-day. This interpretation is supported by the presence of flat bedrock platforms of proposed Miocene age currently situated below sea-level in the Ross Sea Embayment (Fig. 7) (Wilson and Luyendyk 2006). These plateaus are interpreted as having formed by wave erosion at sea-level, yet are currently situated at water depths ranging from *c.* 150 to *c.* 350 m below sea-level, deepening southwards towards the TAM (Wilson and Luyendyk 2006). These observations imply regional subsidence of the Ross Sea Embayment since the Neogene, with a combination

of younger and/or higher magnitude extension towards the TAM. In addition, coring at Deep Sea Drilling Project (DSDP) Site 270 in the Ross Sea (Fig. 7) recovered a terrestrial palaeosol several metres deep developed on a sedimentary breccia above basement gneiss at *c.* 1000 m below sea-level (Ford and Barrett 1975). The palaeosol is overlain by quartz sand and glauconitic greensand, which are dated at *c.*  $26 \pm 1.5$  Ma and interpreted as having been deposited in a near-shore or shallow marine environment (Barrett 1975; De Santis *et al.* 1999; Kulhanek *et al.* 2019). This stratigraphy is consistent with a marine transgression and implies a significant amount of regional subsidence since the early Oligocene.

The first attempt to produce a model of post-Eocene thermal subsidence in the WARS assumed that the rift system comprises five non-overlapping regions, each representing a different phase of the regional extension history (Wilson and Luyendyk 2009). Each phase was assumed to have a uniform stretching factor and an instantaneous age of extension, permitting the use of a simple 1D cooling model (McKenzie 1978) to predict the amount of post-34 Ma thermal subsidence across the WARS. The amount of thermal subsidence ( $S$ ) as a function of time ( $t$ ) is given by (McKenzie 1978)

$$S(t) = \frac{4a\rho_m\alpha T_m}{\pi^2(\rho_m - \rho_i)} \frac{\beta}{\pi} \sin\left(\frac{\pi}{\beta}\right) (1 - e^{-t/\tau}) \quad (3)$$

with

$$\tau = \frac{a^2}{\pi^2\kappa} \quad (4)$$

where  $a$  is the thickness of the lithosphere,  $\alpha$  is the coefficient of thermal expansion,  $T_m$  is the temperature at the base of the lithosphere,  $\kappa$  is the thermal diffusivity of the lithosphere,  $\rho_m$  is the density of the lithospheric mantle,  $\rho_i$  is the density of the material infilling the surface subsidence,  $\beta$  is the stretching factor, and  $\tau$  is thermal decay time constant.

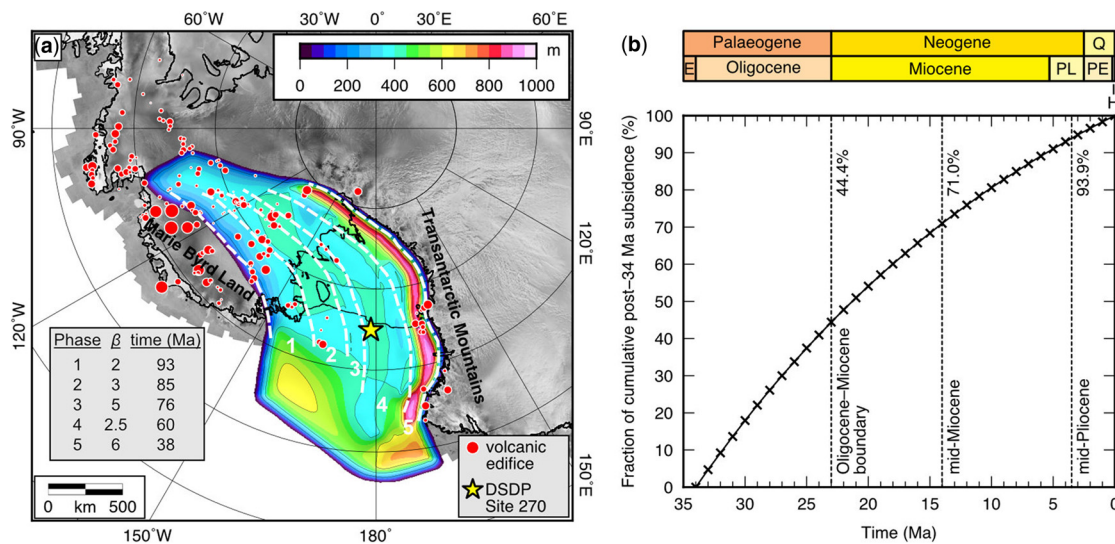


**Fig. 8.** Thermal subsidence in West Antarctica (modified from Paxman *et al.* 2019b). (a) Magnitude of post-34 Ma thermal subsidence associated with the West Antarctic Rift System (Wilson *et al.* 2012; Wilson and Luyendyk 2009). Dashed white lines mark modelled areas of uniform stretching factor ( $\beta$ ) corresponding to five phases of extension in the WARS (Wilson and Luyendyk 2009). The inset table lists the  $\beta$  value and mean age of extension associated with each phase. Filled red circles denote volcanic edifices; circle size is proportional (4x true scale) to the basal diameter of the cone (van Wyk de Vries *et al.* 2018). Yellow star marks the location of Deep Sea Drilling Project (DSDP) Site 270 (Ford and Barrett 1975). (b) Thermal subsidence history since 34 Ma based on a simple 1D cooling model (McKenzie 1978). Cumulative subsidence is measured as a percentage of the total post-34 Ma subsidence; the magnitude of subsidence is spatially variable (see panel a). A simplified geological timescale is provided for reference. Abbreviations: E = Eocene; PL = Pliocene; PE = Pleistocene; H = Holocene; Q = Quaternary.

For their five phases of extension in the WARS, Wilson and Luyendyk (2009) used  $\beta$  factors from 2 to 6 and mean extension ages of 93 to 38 Ma (moving SW from Marie Byrd Land towards the TAM; Fig. 8). This model, with the locus of extension progressively shifting towards the TAM, predicts *c.* 500 m of post-34 Ma subsidence in the central WARS (Fig. 8) (Wilson and Luyendyk 2009). The above rifting parameters were constrained by the necessity to restore the terrestrial palaeosol at DSDP Site 270 to sea-level at *c.* 34 Ma, which required that extension in the central Ross Sea is younger than 70 Ma with a stretching factor of  $>2.0$  (Wilson and Luyendyk 2009; Wilson *et al.* 2012). By correcting for thermal subsidence (following Wilson and Luyendyk 2009), erosion, flooding of the subsided area with water, and associated flexural isostatic responses, the reconstruction process of Wilson *et al.* (2012) produced a substantial upland feature in West Antarctica, with elevations of 500–1000 m above sea-level. The stretching factors also implied a pre-extension crustal thickness of *c.* 50 km in the WARS (Wilson and Luyendyk 2009). These results could be interpreted as lending support to the suggestion that a significant highland plateau and thickened crust existed in West Antarctica prior to extension, of which the Transantarctic Mountains are a remnant (Bialas *et al.* 2007; Huerta 2007). Terrestrial and marine microfossil assemblages obtained via sub-ice drilling near the Siple Coast are indicative of low-elevation coastal plain and shallow marine palaeoenvironments during the Eocene (Coenen *et al.* 2019). This finding contradicts the presence of a uniformly high Siple Coast region during the Eocene (Wilson *et al.* 2012); an alternative scenario is that the palaeotopography was characterized by greater relief, with low-lying areas in the regions now occupied by ice streams and higher terrain in between.

A more recent reconstruction of Antarctic palaeotopography at the Eocene–Oligocene boundary (Paxman *et al.* 2019b) produced palaeo-elevations for the WARS up to 500 m lower than that of Wilson *et al.* (2012). This difference arises from a combination of updated observed offshore sediment volumes and modelled onshore erosion patterns, as

well as updated constraints on the modern regional bedrock topography and  $T_c$ . Use of a simple 1D exponential decay model (McKenzie 1978) to compute the temporal history of thermal subsidence since *c.* 34 Ma (Equation 3; Fig. 8), predicted that DSDP Site 270 subsided below sea-level at *c.* 28 Ma (Paxman *et al.* 2019b), in good agreement with the recorded drill core stratigraphy (Leckie and Webb 1983; Kulhanek *et al.* 2019).

Since many subglacial volcanoes across the WARS may have been emplaced since *c.* 34 Ma, these edifices were removed from the recently updated *c.* 34 Ma palaeotopography (Paxman *et al.* 2019b). The approximate geometry of each volcanic edifice was determined using a recent inventory of the distribution, height, and diameter of subglacial volcanic cones across West Antarctica (Fig. 8) (van Wyk de Vries *et al.* 2018), and these cones were then subtracted from the palaeotopography (Paxman *et al.* 2019b). Since the average diameter of these volcanic cones is 21 km, which is smaller than the flexural length scale of the lithosphere, no flexural isostatic adjustment is required when they are removed from the topography. Moreover, any influence of the edifices (or lack thereof) on past ice sheet dynamics would be highly localized, and largely insignificant within continental-scale ice sheet models with spatial resolutions of  $>10$  km.

#### *Passive continental margins of East Antarctica*

The transient effects of thermal subsidence are not solely pertinent to West Antarctica. During the early Mesozoic, East Antarctica was part of the supercontinent of Gondwana, and was situated in the centre of landmasses that constitute modern-day South America, Africa, Madagascar, India and Australia. Gondwana break-up began in the Jurassic *c.* 180–160 myr ago (Dalziel 1997) with the separation and movement northwards of South America and Africa away from East Antarctica. Break-up then proceeded clockwise around East Antarctica with the successive separation of India and then Australia (Boger 2011 and references therein). East Antarctica

is now bounded by passive margins (Sugden and Jamieson 2018), which are separated from their conjugates in southern Africa, eastern India, and southern Australia by oceanic spreading ridges. These continents each contain Jurassic basalts and dolerite sills formed during volcanic activity associated with the break-up of Gondwana. In Antarctica, these rocks form the Ferrar Large Igneous Province (Elliot and Fleming 2004).

The East Antarctic passive margins would have experienced post-rift thermal subsidence, causing the continental shelves to subside (Hochmuth *et al.* 2020) and providing additional accommodation space for sediments being delivered to the continental margin via erosion and transport by ice or rivers (Jamieson *et al.* 2005, 2008). The break-up age of each sector of the Antarctic margin is well constrained from the age of the oldest sea floor (Müller *et al.* 2016), although the stretching factor and initial timing of continental rifting are more difficult to evaluate. A recent attempt to restore Antarctic margin palaeotopography (since *c.* 34 Ma) for the effects of residual post-rift cooling (Paxman *et al.* 2019b) adopted a 1D cooling model (McKenzie 1978) (equation 3) using the observed age of the sea floor (Müller *et al.* 2016) and a uniform  $\beta$  value of 4 across the widths of the continent–ocean transitions around Antarctica (Gohl 2008). The modelled magnitude of post-Eocene thermal subsidence around the margins of East Antarctica varies from *c.* 300 m for the earliest-formed continental shelves (e.g. offshore Dronning Maud Land), where separation occurred in the Jurassic, to up to *c.* 1200 m for the shelves that experienced separation as recently as the late Cretaceous (e.g. offshore George V Land) (Paxman *et al.* 2019b). However, no firm geological constraints that provide a record of post-Eocene thermal subsidence around the margin of East Antarctica have yet been documented.

### Dynamic topography

Dynamic topography is a collective expression for changes in Earth's surface elevation caused by vertical tractions exerted on the base of the lithosphere by the convecting sub-lithospheric (viscous) mantle (Pekeris 1935; Hager *et al.* 1985; Flament *et al.* 2013; Molnar *et al.* 2015). Convective flow within the mantle is driven by the buoyancy effects of density anomalies, which are in turn caused by variations in temperature and/or composition. When this viscous flow interacts with the surface boundary, viscous normal stresses are generated, causing vertical deflection of the surface. Upward flow towards the surface leads to positive dynamic topography (surface uplift), whereas downward flow away from the surface leads to negative dynamic topography (surface subsidence) (Braun 2010).

Surface manifestations of dynamic topography can range from distributed long-wavelength continental tilting (Sandiford *et al.* 2009; Quigley *et al.* 2010; Richards *et al.* 2016), to more focused surface uplift above the impingement of a mantle plume on the base of the lithosphere (Behrendt *et al.* 1991) or subsidence above a subducting lithospheric slab (Whittaker *et al.* 2010). Ocean floor residual depth measurements from the Southern Ocean reveal dynamic topography amplitudes of up to 1 km and wavelengths of  $10^3$ – $10^4$  km, with spatial variability in magnitude and direction (Hoggard *et al.* 2016, 2017). The temporal pattern of dynamic uplift/subsidence is typically derived from marine stratigraphy, with evidence for typical peak rates on the order of  $100 \text{ m Ma}^{-1}$  (Japsen *et al.* 2006; Al-Hajri *et al.* 2009; Czarnota *et al.* 2013; Richards *et al.* 2016). This implies that long-wavelength changes in bedrock elevation in Antarctica over multi-million year timescales may be attributed, at least in part, to changes in dynamic topography.

### Marie Byrd Land

Marie Byrd Land is defined by a  $1000 \times 500$  km dome-shaped volcanic province (Fig. 7) comprising a series of large shield volcanoes and an extensive sequence of alkali basalts up to *c.* 28–30 Ma in age (LeMasurier *et al.* 1990; Rocchi *et al.* 2006). The geochemistry of basalts in Marie Byrd Land and the WARS is comparable to those found on oceanic islands associated with well-established hot spot tracks (e.g. Hawaii) (LeMasurier and Rex 1989; Hole and LeMasurier 1994), supporting the suggestion of a mantle plume beneath the WARS (Behrendt *et al.* 1991) (see also Bredow and Steinberger 2021). In addition, several low-relief surfaces at scattered localities across Marie Byrd Land with elevations up to 2.7 km have been interpreted as remnants of a continuous, low-relief surface (LeMasurier and Landis 1996). It has been proposed that this erosion surface formed close to base level, and has been uplifted by up to *c.* 2.7 km since *c.* 28–30 Ma, accompanied by block faulting and alkali basalt volcanism, all of which may signal the impingement of a mantle plume on the base of the West Antarctic lithosphere (LeMasurier and Landis 1996).

However, the suggestion of a mantle plume beneath the WARS is controversial; the volume of magmatism imaged within the WARS by geophysical data implies time-averaged magma production rates much lower than those expected for a mantle plume-dominated setting, especially one with relatively thin lithosphere (Rocchi *et al.* 2002). Recent attempts to resolve this controversy have centred on the development of new seismic tomography models for the upper mantle beneath West Antarctica (An *et al.* 2015b; Lloyd *et al.* 2015; Shen *et al.* 2018; Bredow and Steinberger 2021; Wiens *et al.* this 2021). An approximately circular P- and S-wave low-velocity anomaly in the upper mantle would be indicative of a warm thermal anomaly, potentially related to a mantle plume. Such an anomaly is not clearly visible beneath central West Antarctica (An *et al.* 2015a), but may be resolved beneath Marie Byrd Land, although its depth extent is poorly constrained (Fig. 9) (Lloyd *et al.* 2015, 2020; Shen *et al.* 2018). Seismic wave velocities and receiver functions show that the crust beneath the high topography in Marie Byrd Land is up to 10 km thicker than beneath the WARS, indicating that this high topography is at least partially supported isostatically rather than entirely dynamically by a mantle plume (Shen *et al.* 2018). However, satellite gravity gradients show a bowl-shaped structure in Marie Byrd Land, possibly originating from a mantle plume source (Ebbing *et al.* 2018; Pappa and Ebbing 2021).

It is therefore possible, but not conclusively demonstrated, that the long-wavelength, high-elevation domal topography of Marie Byrd Land, anomalous when compared to the adjacent WARS, is in part supported by a hotspot-related thermal anomaly within the upper mantle. If this is the case, understanding the plume-induced topographic evolution of Marie Byrd Land is important for attempts to reconstruct regional palaeotopography. The beginning of Marie Byrd Land uplift was initially assumed to have been contemporaneous with early Oligocene magmatism (*c.* 28–30 Ma) (LeMasurier and Landis 1996), although older volcanic units may have been emplaced but subsequently eroded or not yet sampled. It is possible that dynamic uplift commenced earlier, in response to mantle upwelling during the Cretaceous and early Cenozoic after cessation of subduction following Gondwana break-up (Sutherland *et al.* 2010). Conversely, recent apatite fission track and (U–Th–Sm)/He thermochronology data have been used to tentatively suggest that denudation (and associated uplift) in Marie Byrd Land commenced in the early Miocene (*c.* 20 Ma) (Spiegel *et al.* 2016). However, most low-temperature cooling ages from Marie Byrd Land date to 100–60 Ma, and the 20 Ma age group is based on only two

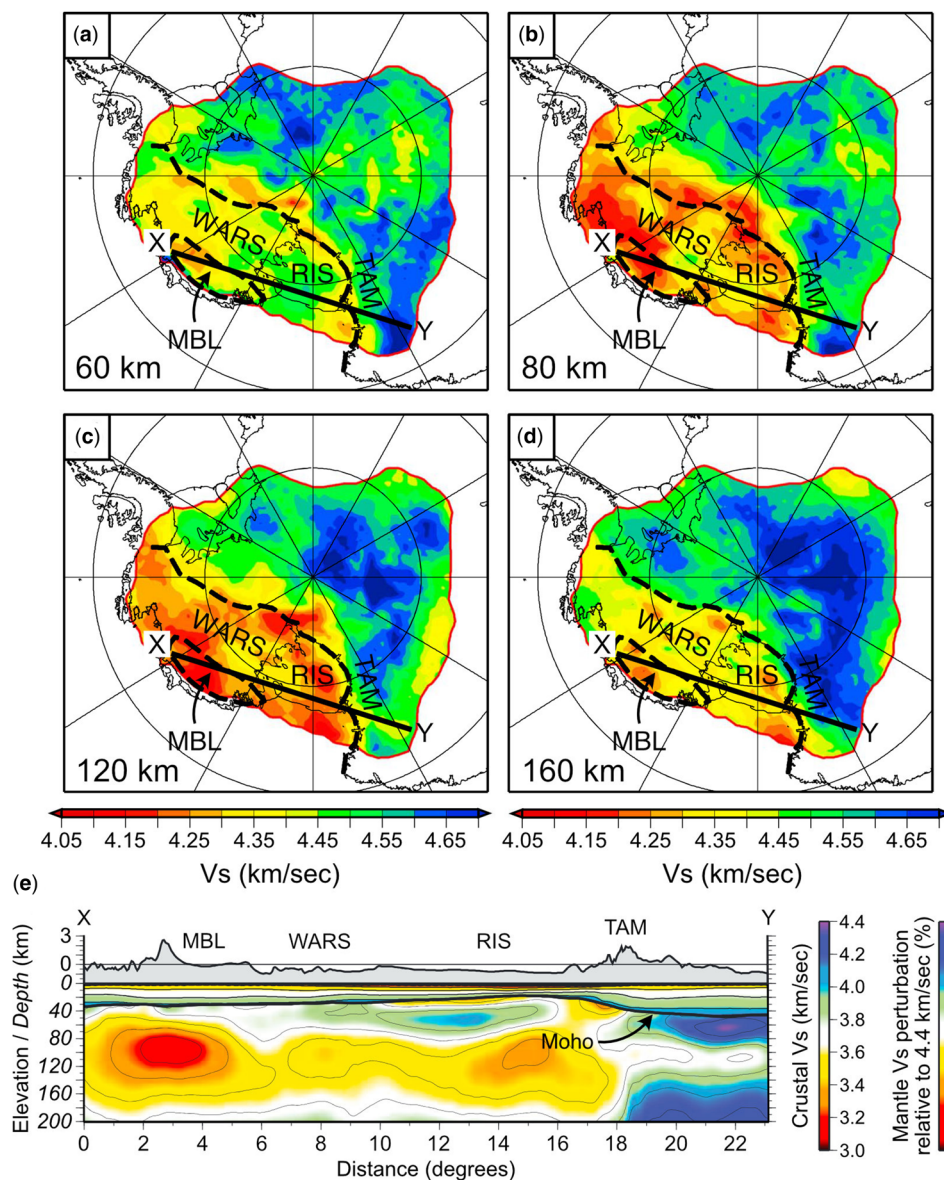


**Fig. 9.** S-wave velocity ( $V_s$ ) model for central and West Antarctica (modified from Shen *et al.* 2018). (a)–(d) Map views of  $V_s$  at four depth slices in the tomography model (depths are relative to a reference datum in the upper crust). Dashed lines mark the approximate limits of Marie Byrd Land and the West Antarctic Rift System. (e) Vertical slice of the 3D tomography model of the crust and upper mantle along transect X–Y (location marked on above panels). The  $V_s$  of the crust is plotted as absolute values, whereas the  $V_s$  of the mantle is shown as percentage perturbation relative to 4.4 km/sec; the Moho is marked by the solid line in the profile. MBL = Marie Byrd Land; RIS = Ross Ice Shelf; TAM = Transantarctic Mountains; WARS = West Antarctic Rift System.

rock samples from one location *c.* 250 km from the centre of the dome (Spiegel *et al.* 2016). Consequently, the questions of whether Marie Byrd Land was uplifted due to mantle plume activity, and the magnitude and timing of any dynamic uplift, remain matters of considerable uncertainty.

Large-scale continental glaciation in coastal West Antarctica would require areas of land situated at significant elevations above sea-level. Marie Byrd Land is therefore a potential candidate for ice sheet inception in West Antarctica. Ice sheet model simulations performed on the palaeotopographical reconstructions of Wilson *et al.* (2012) suggest that the high palaeo-elevations in Marie Byrd Land and central West Antarctica could have permitted the establishment of a significant WAIS at *c.* 34 Ma (Wilson *et al.* 2013). Significant ice still accumulates in the minimum *c.* 34 Ma palaeotopography of Wilson *et al.* (2012), which includes a correction for 1 km of post-34 Ma dynamic uplift in Marie Byrd Land. However, if uplift of up to 2.7 km (LeMasurier and Landis 1996) commenced at *c.* 20 Ma (Spiegel *et al.* 2016), Marie Byrd Land would have been low-lying at *c.* 34 Ma, and regional ice sheet inception may have occurred during the early Miocene at the earliest. This in turn presents a dilemma as to whether/where ice accumulated in West Antarctica during the early Oligocene, which has implications for global ice volumes, sea-level and ocean temperature at this time (Wilson

*et al.* 2013). Since the magnitude of post-Eocene dynamic uplift across Marie Byrd Land may have been anywhere between 0 and 2.7 km, a high degree of uncertainty persists in our understanding of the topographic evolution and glacial history of Marie Byrd Land.

This case study highlights the potential importance of sub-plate processes such as the vertical tractions imposed on the base of the lithosphere by buoyant mantle plumes for the evolution of Antarctic palaeotopography, and in turn for Antarctic glacial history. As well as influencing past ice sheet dynamics via changes in topography, the presence of a mantle plume beneath Marie Byrd Land may also elevate the local geothermal heat flux to values of up to  $150 \text{ mW m}^{-2}$  (Seroussi *et al.* 2017) and, in turn, increase the rate of basal melting beneath the ice sheet, with consequences for ice sheet hydrology (Seroussi *et al.* 2017).

#### Transantarctic Mountains

As outlined in the ‘Flexure and palaeotopography’ section, the origin of the Transantarctic Mountains (TAM) remains a major open question in the history of Antarctica’s subglacial topography. Some studies have proposed that the TAM are isostatically supported by a thickened crust, with gravity

## Antarctic palaeotopography

modelling implying crustal thicknesses *c.* 5–10 km greater than those beneath the Wilkes Subglacial Basin in the immediate hinterland (Studinger *et al.* 2004; Jordan *et al.* 2013). However, although recent seismic studies find a modest (*c.* 5 km) crustal root beneath the TAM, it does not appear to fully support the observed topography (Lawrence *et al.* 2006; Chaput *et al.* 2014; An *et al.* 2015a; Hansen *et al.* 2016; Ramirez *et al.* 2016). The absence of a fully compensating crustal root is more consistent with a flexural origin for the TAM. However, as discussed in the ‘Mechanical unloading and thermal expansion’ section, a problematic observation for the flexure model is that the southern TAM are particularly broad, with a high plateau extending for more than 300 km into East Antarctica (Fretwell *et al.* 2013), which is inconsistent with solely edge-driven flexure at the front of the TAM.

Recently constructed seismic tomographic images of the uppermost mantle beneath the southern TAM reveal a potential mantle source of the observed broad topographic plateau (Shen *et al.* 2017; Wiens *et al.* 2021). Seismically slow uppermost mantle beneath the southern TAM (Fig. 9) is indicative of a hot temperature anomaly capable of reducing the upper mantle density by *c.* 1–1.5%, which would provide sufficient buoyancy to support *c.* 1.5–2.0 km of surface elevation (Shen *et al.* 2017). Tomography images also reveal a fast seismic anomaly beneath the slow uppermost mantle (Fig. 9), which is interpreted as foundering lithosphere that is being replaced at shallow depths by a warmer, wedge-shaped body of asthenosphere (Shen *et al.* 2017, 2018). Cretaceous–Cenozoic rifting within the WARS may have caused thermal destabilization and ultimately delamination of pre-existing cold

lithospheric mantle, thereby triggering lithospheric foundering (Shen *et al.* 2017). Better understanding of the timing of lithospheric foundering and buoyant uplift of the southern TAM plateau is required for more accurate reconstructions of the regional palaeotopography.

## Wilkes Subglacial Basin

The Wilkes Subglacial Basin (WSB) is situated in the immediate hinterland of the TAM (Fig. 2). As a low-lying marine basin containing an ice volume equivalent to *c.* 5 m of global sea-level rise (Fretwell *et al.* 2013; Gasson *et al.* 2015), an understanding of ice sheet behaviour within the WSB during past warmer climates is of particular importance for predicting future ice sheet change in this sector of the East Antarctic Ice Sheet (EAIS). However, significant variation remains between numerical ice sheet model predictions of EAIS retreat within the WSB during past warm periods such as the mid-Pliocene (*c.* 3 Ma) (Pollard and DeConto 2009; Mengel and Levermann 2014; DeConto and Pollard 2016), at which time atmospheric CO<sub>2</sub> levels were similar to that of today (*c.* 400 ppm). Improved understanding of past ice sheet dynamics within the WSB relies in part on understanding the evolution of the subglacial topography of the basin (Paxman *et al.* 2018).

Austermann *et al.* (2015) used the ‘ASPECT’ mantle convection code (Bredow and Steinberger 2021) to model changes in dynamic topography in the WSB since the mid-Pliocene (Fig. 10). The present-day dynamic topography field was computed from the modern density and viscosity

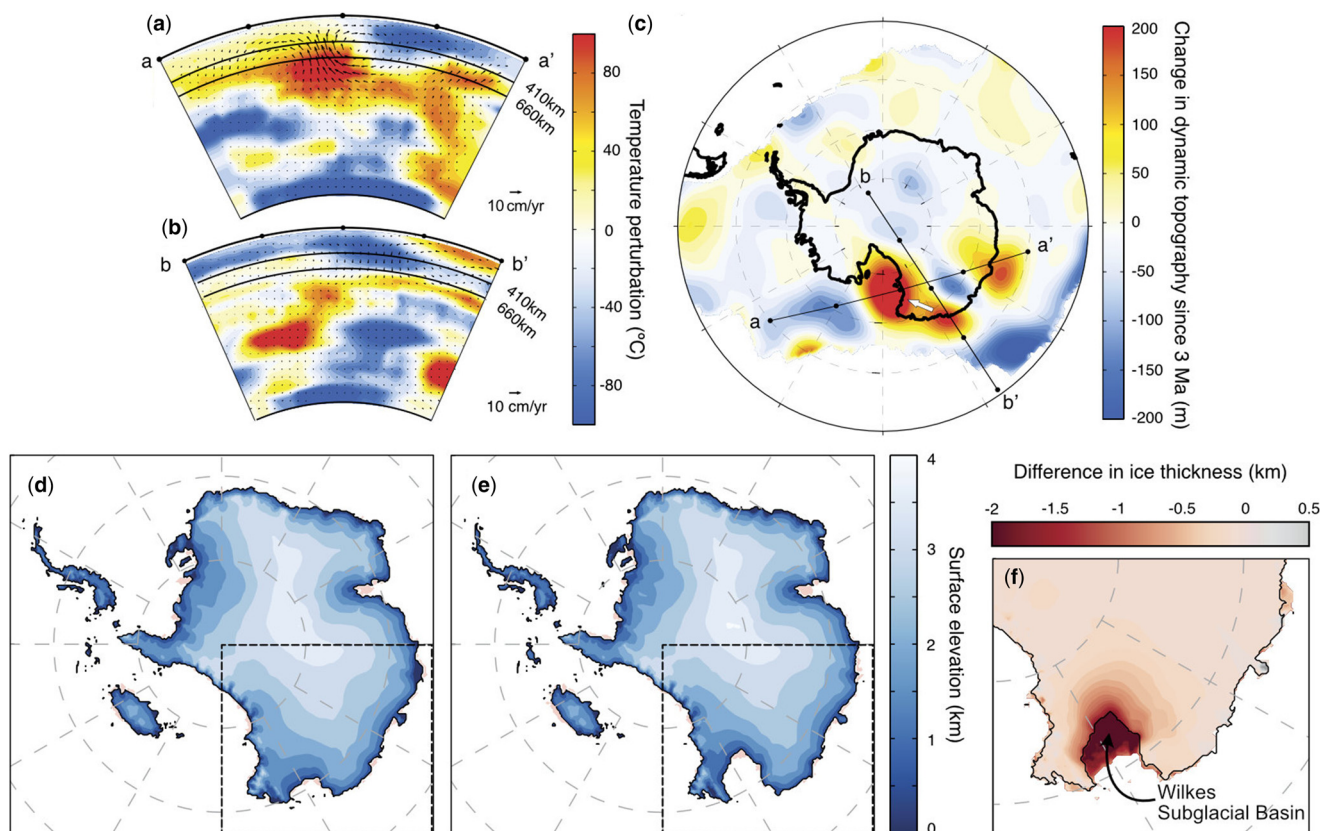


**Fig. 10.** Mantle flow, dynamic topography, and ice sheet modelling in the Wilkes Subglacial Basin (modified from Austermann *et al.* 2015). (a) and (b) Present-day mantle temperature fields (perturbations relative to the global average) and computed mantle flow vectors for transects a–a' and b–b' crossing the Wilkes Subglacial Basin (profile locations indicated in panel c). (c) Change in dynamic topography since 3 Ma caused by the motion of the Antarctic plate through the mantle flow field. The plate rotation vector in the Wilkes Subglacial Basin is marked by white arrow, and has a magnitude of 1.6 cm/yr. (d) and (e) AIS surface elevation computed using simulations for mid-Pliocene climates which (d) do not include, and (e) do include, changes in dynamic topography since 3 Ma (panel c). (f) Difference in ice sheet thickness in the Wilkes Subglacial Basin (panel extent marked by dashed boxes in panels d and e) between the simulations shown in panels d and e.

structure of the mantle (as constrained from seismic tomography and mineral physics). Changes in local dynamic topography were assumed to arise entirely from the motion of the Antarctic plate through this dynamic topography field (Austermann *et al.* 2015). This combined mantle flow and plate motion modelling approach predicted that the bed of the northern WSB (close to the present-day ice margin) was *c.* 100–200 m lower during the mid-Pliocene than today (Fig. 10) (Austermann *et al.* 2015). Incorporating this change in bed elevation into an ice sheet model (Pollard and DeConto 2009) resulted in an additional 200–560 km of grounding line retreat into the WSB under a mid-Pliocene climate (Fig. 10) (Austermann *et al.* 2015). The implication is that a relatively modest amount of dynamic uplift of the WSB since 3 Ma has acted to significantly increase the stability of this sector of the EAIS.

Austermann *et al.* (2015) also computed the change in dynamic topography across the entirety of Antarctica since 3 Ma (Fig. 10) and found that the amplitude of dynamic topography change in other marine-based sectors of the EAIS, such as the Aurora or Recovery subglacial basins, was relatively small by comparison to the WSB, with little impact on ice sheet behaviour. This study calculates the mantle flow field from the present-day density and viscosity structure of the mantle. Constraining these parameters – and the mantle flow field – in the geological past is particularly challenging, especially in Antarctica, and results in large uncertainties in predictions of changes in dynamic topography over multi-million-year timescales. Moreover, numerical mantle convection models tend to over-predict the amplitudes of dynamic topography measured from (e.g.) residual depth anomalies in the oceanic realm (Hoggard *et al.* 2016), indicating that mantle flow models alone cannot yet be relied upon to reliably correct for dynamic topography changes.

#### Antarctic-wide dynamic topography

Aside from the use of mantle flow simulations, separate attempts have been made to constrain continental-scale patterns of dynamic topography in Antarctica using geophysical datasets. For example, the seismic crustal thickness can be used to calculate surface elevations that would result if topography were entirely supported by variations in crustal thickness (Airy isostasy; ‘Elastic plate flexure’ section).

$$h_{\text{isostatic}} = \frac{(\rho_m - \rho_c)}{\rho_m} (T_c - T_0) \quad (5)$$

where  $T_c$  is the observed crustal thickness,  $T_0$  is the zero-elevation crustal thickness,  $\rho_m$  is the density of the mantle,  $\rho_c$  is the density of the crust, and  $h_{\text{isostatic}}$  is the ‘isostatic topography’ – that is, the topography supported by isostatic buoyancy forces. The isostatic topography can be subtracted from the observed topography to give a ‘residual topography’, which may be, to some extent, supported by vertical tractions applied to the base of the lithosphere by the convecting mantle (Menard 1973; Cazenave *et al.* 1989; Forte *et al.* 1993; Molnar *et al.* 2015).

Comparison of Antarctica’s observed bedrock topography (Fretwell *et al.* 2013) with the computed isostatic topography indicates that local crustal thickening beneath the highlands of the Gamburtsev Subglacial Mountains and Dronning Maud Land can support their differential elevation above the broader East Antarctic plateau (Fig. 11) (O’Donnell and Nyblade 2014). However, the modal elevations of the plateau itself are *c.* 700 m higher than can be accounted for based on its crustal thickness relative to that of the rest of East Antarctica (Fig. 11) (O’Donnell and Nyblade

2014). This Airy isostatic deficit beneath the East Antarctic plateau is also noted from Moho depths derived from gravity inversions (Pappa *et al.* 2019; Pappa and Ebbing this volume). Both studies speculate that this anomalous topography may be supported by a mid-to-lower mantle source, and is therefore ‘dynamic’ (O’Donnell and Nyblade 2014; Pappa *et al.* 2019).

However, calculations attempting to separate isostatic and dynamic topography are subject to a number of uncertainties:

1. Isostatic topography is calculated assuming an Airy model of isostasy, and so does not account for elastic plate flexure (see ‘Elastic plate flexure’ section).
2. Crustal thickness observations are often unreliable or associated with large uncertainties. In Antarctica, crustal thickness is either estimated from satellite gravity inversion models (Block *et al.* 2009; Pappa *et al.* 2019; Pappa and Ebbing 2021) or from seismic receiver functions (Hansen *et al.* 2010; An *et al.* 2015a; Wiens *et al.* 2021), which are typically associated with uncertainties of at least  $\pm 4$  km, which translate into uncertainties of  $\pm c.$  700 m in the isostatic topography.
3. The density contrast between the lower crust and the lithospheric mantle is often also associated with large uncertainty.

Gravity anomalies, rather than crustal thickness measurements, are considered by several authors to offer the tightest constraints on dynamic topography in the continents (McKenzie 2010; Molnar *et al.* 2015). Numerical models of convective mantle flow indicate that the expected ratio between the ‘dynamic’ free-air anomaly and topography (the ‘convective admittance’) is *c.* 30 mGal km<sup>-1</sup> for water/ice-covered terrain (McKenzie *et al.* 1974; McKenzie 1994). This ‘rule’ for converting free-air anomalies into dynamically supported topography is generally supported by limited observations in the oceanic realm (Winterbourne *et al.* 2014; Hoggard *et al.* 2017). The long-wavelength gravity field (>3300 km; Watts and Moore 2017) can therefore be scaled using the convective admittance to produce an estimate of dynamic topography (Fig. 11) (Hoggard *et al.* 2016, 2017).

However, this approach has not so far been used for Antarctica, and there are reasons to exercise caution with its application. Recent models of mantle convection show that the sensitivity kernels for gravity and topography are different, such that the relationship between ‘dynamic’ gravity and topography is not summarized by a constant admittance, but one which is a function of the wavelength and depth of the driving buoyancy anomaly (Colli *et al.* 2016). Sizeable dynamic topography may therefore exist without a corresponding gravity anomaly, and vice versa. Indeed, the correlation between residual topography (from crustal thickness measurements) and dynamic gravity is generally poor (Fig. 11).

The spatial and temporal evolution of the amplitude and direction of changes in dynamic topography in Antarctica since *c.* 34 Ma remain poorly understood. Development of an Antarctic palaeo-dynamic topography model will require an expanded coverage of seismic stations in Antarctica, and a reduction in the epistemic uncertainty within mantle flow models. Also required is the identification of readily dated geological markers that can constrain the magnitude and pattern of dynamic uplift or subsidence on length scales of hundreds to thousands of kilometres, although such exposure does not exist in Antarctica. These limitations and uncertainties become increasingly problematic when moving further back in time, which makes reconstructing changes in dynamic topography over the course of Antarctica’s glacial history (since *c.* 34 Ma) particularly challenging.

## Antarctic palaeotopography

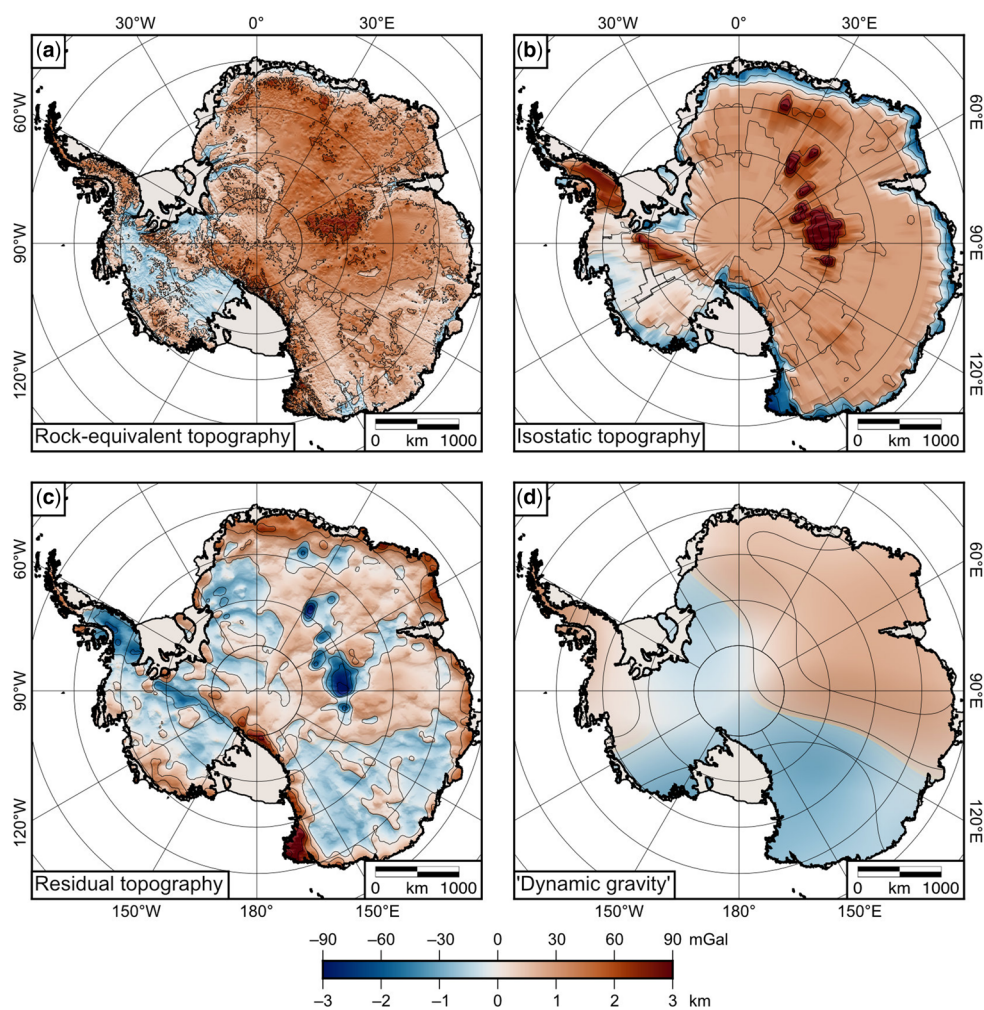


**Fig. 11.** Compensation of topography in Antarctica. (a) Present-day ‘rock-equivalent’ topography, whereby the ice sheet is converted into an equivalent mass of rock and added to the bed topography. Elevations are relative to mean sea-level. (b) Isostatic topography, calculated from the seismic crustal thickness assuming local compensation (Airy isostasy) and a zero-elevation crustal thickness of 35 km for East Antarctica and 25 km for West Antarctica (An *et al.* 2015a). (c) Residual topography, calculated by subtracting the isostatic topography from the rock-equivalent topography. This represents topography that is not in Airy isostatic balance. While this imbalance may be due to dynamic support of topography by the mantle, it may arise due to flexural isostasy or variations in crustal density. The topography has been median filtered at 100 km to remove short-wavelength features unlikely to arise from mantle convection. (d) Long-wavelength (>3300 km) GOCE satellite gravity anomaly (Bruinsma *et al.* 2014), which is scaled to dynamic topography using a uniform ‘convective’ admittance ratio of 30 mGal/km.

## Conclusions

The preceding sections have illustrated the influences of the Antarctic mantle on palaeotopography. The ‘Isostasy’ section illustrated how lithospheric flexure has acted to increase (ice-free) bed elevations in regions subjected to unloading of the lithosphere via glacial erosion, extensional faulting, and conduction of heat within the lithosphere (Fig. 6). The third section, ‘Thermal subsidence’, highlighted the role of protracted lithospheric cooling in Antarctica, primarily in the West Antarctic Rift System. The result has been gradual topographic subsidence of up to 1 km since *c.* 34 Ma (Fig. 8) (Wilson and Luyendyk 2009). The fourth section, ‘Dynamic topography’, showed that it remains difficult to evaluate long-term changes in mantle convection and dynamic topography over geological timescales in Antarctica, despite recent modelling results from the Wilkes Subglacial Basin (Fig. 10) (Austermann *et al.* 2015).

The nature of the Antarctic mantle, and its role in the evolution of subglacial topography, has a number of implications for the past behaviour of the AIS.

1. Early Antarctic ice sheets likely exploited pre-existing tectonic structures such as fault systems and their associated topography. Subsequent excavation of deep subglacial troughs and associated flexural uplift of the trough flanks facilitated effective focussing of glacial flow and erosion within the troughs and contemporaneous preservation of the adjacent highlands beneath non-erosive ice. The patterns of glacial erosion and flexural uplift are therefore governed in part by pre-existing structural

weaknesses within, and the flexural rigidity of, the Antarctic lithosphere.

2. Reconstructions of palaeotopography at *c.* 34 Ma have significantly less area below sea-level and much shallower marine basins than the modern topography (Wilson *et al.* 2012; Paxman *et al.* 2019b). This is largely due to bed overdeepening by glacial erosion (see above), and subsidence driven by post-rift lithospheric cooling. Widespread subsidence of up to 1 km in West Antarctica (Wilson and Luyendyk 2009; Wilson *et al.* 2012) has resulted in the development of an extensive area of low-lying, reverse-sloping topography beneath the WAIS. Landscape evolution models indicate that much of West Antarctica had subsided below sea-level by the mid-Miocene (*c.* 14 Ma) (Paxman *et al.* 2019b). The WAIS may therefore have become increasingly sensitive to marine ice sheet instability processes and associated rapid and irreversible losses of ice volume after this time. In addition, the progressive deepening of topography in East Antarctica by structurally steered glacial erosion during the past 34 Myr may have also facilitated an increase in the sensitivity of the EAIS to climate and ocean forcing (Paxman *et al.* 2020).
3. Changes in dynamic topography of as little as 100–200 m have potentially induced significant changes in ice sheet sensitivity in the Wilkes Subglacial Basin since as recently as the mid-Pliocene (*c.* 3 Ma) (Austermann *et al.* 2015). Considerable uncertainty remains, however, regarding the spatial and temporal evolution of Antarctic dynamic topography through the Cenozoic, with potentially major ramifications for ice sheet stability and sea-level change.

Overall, palaeotopographic reconstructions and ice sheet models suggest that the evolution of the subglacial topography of Antarctica has important implications for past Antarctic ice sheet behaviour (and in turn global sea-levels), in terms of the extent and rate of (i) ice growth during cold climate intervals, and (ii) ice loss during warm climate intervals (Wilson *et al.* 2013; Gasson *et al.* 2016; Colleoni *et al.* 2018). This modification of the subglacial landscape and associated impact on ice sheet behaviour can be attributed to interactions and feedbacks between surface, crustal, and mantle processes, such as glacial erosion, faulting, flexure, thermal subsidence, and dynamic topography. An improved understanding of mantle properties and processes, including in particular (a) a more robust model of the flexural rigidity of Antarctica's lithosphere, (b) further constraints on the pattern of rifting and thermal subsidence in West Antarctica and around the margins of East Antarctica, and (c) a better understanding of changes in mantle convection patterns and associated changes dynamic topography, on the evolution of Antarctic palaeotopography is therefore a key priority in the next generation of Antarctic landscape evolution and ice sheet models.

**Acknowledgements** Many of the topics described in this chapter are based on contributions from the ANTscape working group within the Past Antarctic Ice Sheet dynamics (PAIS) research programme of the Scientific Committee on Antarctic Research (SCAR). I would like to acknowledge the support of the major contributors to this programme, including Peter Barrett, Graeme Eagles, Karsten Gohl, Katharina Hochmuth, Stewart Jamieson, German Leitchenkov, Doug Wilson, and the numerous attendees of the various ANTscape workshops on Antarctic palaeotopography and palaeobathymetry that were instrumental in the development of several concepts reviewed in this chapter. I would also like to extend thanks to Mark Hoggard and Doug Wilson for their thorough and constructive reviews, which greatly improved the quality of this chapter.

**Author contributions** GJGP: writing – original draft (lead), writing – review & editing (lead).

**Funding** The author would like to acknowledge the support of a Natural Environment Research Council UK studentship (NE/L002590/1).

**Data availability** Data sharing is not applicable to this article as no datasets were generated or analysed during the current study.

## References

- Aitken, A.R.A., Roberts, J.L. *et al.* 2016. Repeated large-scale retreat and advance of Totten Glacier indicated by inland bed erosion. *Nature*, **533**, 385–389, <https://doi.org/10.1038/nature17447>
- Al-Hajri, Y., White, N. and Fishwick, S. 2009. Scales of transient convective support beneath Africa. *Geology*, **37**, 883–886, <https://doi.org/10.1130/G25703A.1>
- An, M., Wiens, D.A. *et al.* 2015a. S-velocity model and inferred Moho topography beneath the Antarctic Plate from Rayleigh waves. *Journal of Geophysical Research Solid Earth*, **120**, 359–383, <https://doi.org/10.1002/2014JB011332>
- An, M., Wiens, D.A. *et al.* 2015b. Temperature, lithosphere–asthenosphere boundary, and heat flux beneath the Antarctic Plate inferred from seismic velocities. *Journal of Geophysical Research Solid Earth*, **120**, 8720–8742, <https://doi.org/10.1002/2015JB011917>
- Austermann, J., Pollard, D. *et al.* 2015. The impact of dynamic topography change on Antarctic ice sheet stability during the mid-Pliocene warm period. *Geology*, **43**, 927–930, <https://doi.org/10.1130/G36988.1>
- Barletta, V.R., Bevis, M. *et al.* 2018. Observed rapid bedrock uplift in Amundsen Sea Embayment promotes ice-sheet stability. *Science*, **360**, 1335–1339, <https://doi.org/10.1126/science.124447>
- Barrett, P.J. 1975. Textural characteristics of Cenozoic preglacial and glacial sediments at Site 270, Ross Sea, Antarctica. *Initial Reports of the Deep Sea Drilling Project Leg 28*, **28**, 757–767.
- Barrett, P.J. 2008. A history of antarctic cenozoic glaciation – view from the margin. In: Florindo, F. and Siebert, M.J. (eds) *Developments in Earth and Environmental Sciences*. Elsevier, 33–83, [https://doi.org/10.1016/S1571-9197\(08\)00003-7](https://doi.org/10.1016/S1571-9197(08)00003-7)
- Behrendt, J.C., LeMasurier, W.E., Cooper, A.K., Tessensohn, F., Tréhu, A. and Damaske, D. 1991. Geophysical studies of the West Antarctic Rift System. *Tectonics*, **10**, 1257–1273, <https://doi.org/10.1029/91TC00868>
- Behrendt, J.C., Blankenship, D.D., Finn, C.A., Bell, R.E., Sweeney, R.E., Hodge, S.M. and Brozena, J.M. 1994. CASERTZ aeromagnetic data reveal late Cenozoic flood basalts(?) in the West Antarctic rift system. *Geology*, **22**, 527, [https://doi.org/10.1130/0091-7613\(1994\)022<0527:CADRLC>2.3.CO;2](https://doi.org/10.1130/0091-7613(1994)022<0527:CADRLC>2.3.CO;2)
- Bell, R.E., Blankenship, D.D., Finn, C.A., Morse, D.L., Scambos, T.A., Brozena, J.M. and Hodge, S.M. 1998. Influence of subglacial geology on the onset of a West Antarctic ice stream from aerogeophysical observations. *Nature*, **394**, 58–62, <https://doi.org/10.1038/27883>
- Bentley, M.J., O’Cofaigh, C. *et al.* 2014. A community-based geological reconstruction of Antarctic Ice Sheet deglaciation since the Last Glacial Maximum. *Quaternary Science Reviews*, **100**, 1–9, <https://doi.org/10.1016/j.quascirev.2014.06.025>
- Bialas, R.W., Buck, W.R., Studinger, M. and Fitzgerald, P.G. 2007. Plateau collapse model for the Transantarctic Mountains–West Antarctic Rift System: insights from numerical experiments. *Geology*, **35**, 687–690, <https://doi.org/10.1130/G23825A.1>
- Bingham, R.G., Ferraccioli, F., King, E.C., Larter, R.D., Pritchard, H.D., Smith, A.M. and Vaughan, D.G. 2012. Inland thinning of West Antarctic Ice Sheet steered along subglacial rifts. *Nature*, **487**, 468–471, <https://doi.org/10.1038/nature11292>
- Block, A.E., Bell, R.E. and Studinger, M. 2009. Antarctic crustal thickness from satellite gravity: implications for the Transantarctic and Gamburtsev Subglacial Mountains. *Earth and Planetary Science Letters*, **288**, 194–203, <https://doi.org/10.1016/j.epsl.2009.09.022>
- Boger, S.D. 2011. Antarctica – before and after Gondwana. *Gondwana Research*, **19**, 335–371, <https://doi.org/10.1016/j.gr.2010.09.003>
- Braun, J. 2010. The many surface expressions of mantle dynamics. *Nature Geoscience*, **3**, 825–833, <https://doi.org/10.1038/ngeo1020>
- Bredow, E. and Steinberger, B. 2021. Mantle convection and possible mantle plumes beneath Antarctica: insights from geodynamic models and implications for topography. *Geological Society, London, Memoirs*, **56**, <https://doi.org/10.1144/M56-2020-2>
- Brenn, G.R., Hansen, S.E. and Park, Y. 2017. Variable thermal loading and flexural uplift along the Transantarctic Mountains, Antarctica. *Geology*, **45**, 463–466, <https://doi.org/10.1130/G38784.1>
- Bruinsma, S.L., Förste, C. *et al.* 2014. ESA’s satellite-only gravity field model via the direct approach based on all GOCE data. *Geophysical Research Letters*, **41**, 7508–7514, <https://doi.org/10.1002/2014GL062045>
- Burton-Johnson, A., Black, M., Peter, T.F. and Kaluza-Gilbert, J. 2016. An automated methodology for differentiating rock from snow, clouds and sea in Antarctica from Landsat 8 imagery: a new rock outcrop map and area estimation for the entire Antarctic continent. *Cryosphere*, **10**, 1665–1677, <https://doi.org/10.5194/tc-10-1665-2016>
- Cande, S.C., Stock, J.M., Müller, R.D. and Ishihara, T. 2000. Cenozoic motion between East and West Antarctica. *Nature*, **404**, 145–150, <https://doi.org/10.1038/35004501>
- Carter, A., Riley, T.R., Hillenbrand, C.-D. and Rittner, M. 2017. Widespread Antarctic glaciation during the Late Eocene. *Earth*

## Antarctic palaeotopography

- and *Planetary Science Letters*, **458**, 49–57, <https://doi.org/10.1016/j.epsl.2016.10.045>
- Cazenave, A., Souriau, A. and Dominh, K. 1989. Global coupling of Earth surface topography with hotspots, geoid and mantle heterogeneities. *Nature*, **340**, 54–57, <https://doi.org/10.1038/340054a0>
- Chaput, J., Aster, R.C. *et al.* 2014. The crustal thickness of West Antarctica. *Journal of Geophysical Research Solid Earth*, **119**, 378–395, <https://doi.org/10.1002/2013JB010642>
- Chen, B., Haeger, C., Kaban, M.K. and Petrunin, A.G. 2018. Variations of the effective elastic thickness reveal tectonic fragmentation of the Antarctic lithosphere. *Tectonophysics*, **746**, 412–424, <https://doi.org/10.1016/j.tecto.2017.06.012>
- Clerc, F., Minchew, B.M. and Behn, M.D. 2019. Marine ice cliff instability mitigated by slow removal of ice shelves. *Geophysical Research Letters*, **46**, 12108–12116, <https://doi.org/10.1029/2019GL084183>
- Coenen, J.J., Scherer, R., Baudoin, P., Warny, S., Castañeda, I.S. and Askin, R. 2019. Paleogene marine and terrestrial development of the West Antarctic Rift System. *Geophysical Research Letters*, **47**, <https://doi.org/10.1029/2019GL085281>
- Colleoni, F., De Santis, L. *et al.* 2018. Past continental shelf evolution increased Antarctic ice sheet sensitivity to climatic conditions. *Scientific Reports*, **8**, 11323, <https://doi.org/10.1038/s41598-018-29718-7>
- Colli, L., Ghelichkhan, S. and Bunge, H.P. 2016. On the ratio of dynamic topography and gravity anomalies in a dynamic Earth. *Geophysical Research Letters*, **43**, 2510–2516, <https://doi.org/10.1002/2016GL067929>
- Cox, S.E., Thomson, S.N., Reiners, P.W., Hemming, S.R. and van de Fliedert, T. 2010. Extremely low long-term erosion rates around the Gamburtsev Mountains in interior East Antarctica. *Geophysical Research Letters*, **37**, <https://doi.org/10.1029/2010GL045106>
- Coxall, H.K., Wilson, P.A., Pälike, H., Lear, C.H. and Backman, J. 2005. Rapid stepwise onset of Antarctic glaciation and deeper calcite compensation in the Pacific Ocean. *Nature*, **433**, 53–57, <https://doi.org/10.1038/nature03135>
- Czarnota, K., Hoggard, M.J., White, N. and Winterbourne, J., 2013. Spatial and temporal patterns of Cenozoic dynamic topography around Australia. *Geochemistry, Geophysics Geosystems*, **14**, 634–658, <https://doi.org/10.1029/2012GC004392>
- Dalziel, I.W.D. 1997. Neoproterozoic–Paleozoic geography and tectonics: review, hypothesis, environmental speculation. *Geological Society of America Bulletin*, **109**, 16–42, [https://doi.org/10.1130/0016-7606\(1997\)109<0016:ONPGAT>2.3.CO;2](https://doi.org/10.1130/0016-7606(1997)109<0016:ONPGAT>2.3.CO;2)
- De Santis, L., Prato, S., Brancolini, G., Lovo, M. and Torelli, L. 1999. The Eastern Ross Sea continental shelf during the Cenozoic: implications for the West Antarctic ice sheet development. *Global and Planetary Change*, **23**, 173–196, [https://doi.org/10.1016/S0921-8181\(99\)00056-9](https://doi.org/10.1016/S0921-8181(99)00056-9)
- Decesari, R.C., Wilson, D.S., Luyendyk, B.P. and Faulkner, M. 2007. Cretaceous and Tertiary extension throughout the Ross Sea, Antarctica. In: Cooper, A.K. (ed.) *Antarctica: A Keystone in a Changing World – Online Proceedings of the 10th ISAES*. US Geological Survey. Open File Rep., 2007-1047, <https://doi.org/10.3133/of2007-1047.srp098>
- DeConto, R.M. and Pollard, D. 2003a. Rapid Cenozoic glaciation of Antarctica induced by declining atmospheric CO<sub>2</sub>. *Nature*, **421**, 245–249, <https://doi.org/10.1038/nature01290>
- DeConto, R.M. and Pollard, D. 2003b. A coupled climate–ice sheet modeling approach to the Early Cenozoic history of the Antarctic ice sheet. *Palaeogeography Palaeoclimatology Palaeoecology*, **198**, 39–52, [https://doi.org/10.1016/S0031-0182\(03\)00393-6](https://doi.org/10.1016/S0031-0182(03)00393-6)
- DeConto, R.M. and Pollard, D. 2016. Contribution of Antarctica to past and future sea-level rise. *Nature*, **531**, 591–597, <https://doi.org/10.1038/nature17145>
- DeConto, R.M., Pollard, D., Wilson, P.A., Pälike, H., Lear, C.H. and Pagani, M. 2008. Thresholds for Cenozoic bipolar glaciation. *Nature*, **455**, 652–656, <https://doi.org/10.1038/nature07337>
- Drewry, D.J. 1983. *Antarctica: Glaciological and Geophysical Folio*. Scott Polar Research Institute, University of Cambridge.
- Ebbing, J., Haas, P., Ferraccioli, F., Pappa, F., Szwillus, W. and Bouman, J. 2018. Earth tectonics as seen by GOCE - Enhanced satellite gravity gradient imaging. *Scientific Reports*, **8**, 16356, <https://doi.org/10.1038/s41598-018-34733-9>
- Edwards, T.L., Brandon, M.A. *et al.* 2019. Revisiting Antarctic ice loss due to marine ice-cliff instability. *Nature*, **566**, 58–64, <https://doi.org/10.1038/s41586-019-0901-4>
- Elliot, D.H. and Fleming, T.H. 2004. Occurrence and dispersal of magmas in the Jurassic Ferrar Large Igneous Province, Antarctica. *Gondwana Research*, **7**, 223–237, [https://doi.org/10.1016/S1342-937X\(05\)70322-1](https://doi.org/10.1016/S1342-937X(05)70322-1)
- Ferraccioli, F., Armadillo, E., Zunino, A., Bozzo, E., Rocchi, S. and Armienti, P. 2009. Magmatic and tectonic patterns over the Northern Victoria Land sector of the Transantarctic Mountains from new aeromagnetic imaging. *Tectonophysics*, **478**, 43–61, <https://doi.org/10.1016/j.tecto.2008.11.028>
- Ferraccioli, F., Finn, C.A., Jordan, T.A., Bell, R.E., Anderson, L.M. and Damaske, D. 2011. East Antarctic rifting triggers uplift of the Gamburtsev Mountains. *Nature*, **479**, 388–392, <https://doi.org/10.1038/nature10566>
- Finn, C.A., Müller, R.D. and Panter, K.S. 2005. A Cenozoic diffuse alkaline magmatic province (DAMP) in the southwest Pacific without rift or plume origin. *Geochemistry, Geophysics Geosystems*, **6**, <https://doi.org/10.1029/2004GC000723>
- Flament, N., Gurnis, M. and Muller, R.D. 2013. A review of observations and models of dynamic topography. *Lithosphere*, **5**, 189–210, <https://doi.org/10.1130/L245.1>
- Ford, A.B. and Barrett, P.J. 1975. Basement rocks of the south-central Ross Sea, Site 270, DSDP Leg 28. *Initial Reports of the Deep Sea Drilling Project Leg 28*, **28**, 861–868.
- Forsberg, R., Olesen, A.V. *et al.* 2018. Exploring the Recovery Lakes region and interior Dronning Maud Land, East Antarctica, with airborne gravity, magnetic and radar measurements. *Geological Society, London, Special Publications*, **461**, <https://doi.org/10.1144/SP461.17>
- Forte, A.M., Peltier, W.R., Dziewonski, A.M. and Woodward, R.L. 1993. Dynamic surface topography: a new interpretation based upon mantle flow models derived from seismic tomography. *Geophysical Research Letters*, **20**, 225–228, <https://doi.org/10.1029/93GL00249>
- Fretwell, P., Pritchard, H.D. *et al.* 2013. Bedmap2: improved ice bed, surface and thickness datasets for Antarctica. *Cryosphere*, **7**, 375–393, <https://doi.org/10.5194/tc-7-375-2013>
- Gasson, E., DeConto, R.M. and Pollard, D. 2015. Antarctic bedrock topography uncertainty and ice sheet stability. *Geophysical Research Letters*, **42**, 5372–5377, <https://doi.org/10.1002/2015GL064322>
- Gasson, E., DeConto, R.M., Pollard, D. and Levy, R.H. 2016. Dynamic Antarctic ice sheet during the early to mid-Miocene. *Proceedings of the National Academy of Sciences*, **113**, 3459–3464, <https://doi.org/10.1073/pnas.1516130113>
- Gohl, K. 2008. Antarctica's continent-ocean transitions: consequences for tectonic reconstructions. In: Cooper, A.K., Barrett, P.J., Stagg, H.M.J., Storey, B.C., Stump, E. and Wise, W. (eds) *Antarctica: A Keystone in a Changing World – Online Proceedings of the 10th ISAES*. The National Academies Press, Washington, DC, 29–38, <https://doi.org/10.3133/of2007-1047.kp04>
- Golledge, N.R., Kowalewski, D.E., Naish, T.R., Levy, R.H., Fogwill, C.J. and Gasson, E.G.W. 2015. The multi-millennial Antarctic commitment to future sea-level rise. *Nature*, **526**, 421–425, <https://doi.org/10.1038/nature15706>
- Gomez, N., Mitrovica, J.X., Huybers, P. and Clark, P.U. 2010. Sea level as a stabilizing factor for marine-ice-sheet grounding lines. *Nature Geoscience*, **3**, 850–853, <https://doi.org/10.1038/ngeo1012>
- Granot, R. and Dymet, J. 2018. Late Cenozoic unification of East and West Antarctica. *Nature Communications*, **9**, 3189, <https://doi.org/10.1038/s41467-018-05270-w>
- Hager, B.H., Clayton, R.W., Richards, M.A., Comer, R.P. and Dziewonski, A.M. 1985. Lower mantle heterogeneity, dynamic

- topography and the geoid. *Nature*, **314**, 752–752, <https://doi.org/10.1038/314752a0>
- Hambrey, M.J., Ehrmann, W.U. and Larsen, B. 1991. Cenozoic Glacial Record of the Prydz Bay Continental Shelf, East Antarctica. *Proceedings of the Ocean Drilling Program, Scientific Results*, **119**, 77–132, <https://doi.org/10.2973/odp.proc.sr.119.200.1991>
- Hansen, S.E., Nyblade, A.A., Heeszel, D.S., Wiens, D.A., Shore, P. and Kanao, M. 2010. Crustal structure of the Gamburtsev Mountains, East Antarctica, from S-wave receiver functions and Rayleigh wave phase velocities. *Earth and Planetary Science Letters*, **300**, 395–401, <https://doi.org/10.1016/j.epsl.2010.10.022>
- Hansen, S.E., Kenyon, L.M., Graw, J.H., Park, Y. and Nyblade, A.A. 2016. Crustal structure beneath the Northern Transantarctic Mountains and Wilkes Subglacial Basin: implications for tectonic origins. *Journal of Geophysical Research Solid Earth*, **121**, 812–825, <https://doi.org/10.1002/2015JB012325>
- Hochmuth, K., Gohl, K. *et al.* 2020. The evolving paleobathymetry of the Circum-Antarctic Southern Ocean since 34 Ma: a key to understanding past cryosphere-ocean developments. *Geochemistry, Geophysics, Geosystems*, **21**.
- Hoggard, M.J., White, N. and Al-Attar, D. 2016. Global dynamic topography observations reveal limited influence of large-scale mantle flow. *Nature Geoscience*, **9**, 456–463, <https://doi.org/10.1038/ngeo2709>
- Hoggard, M.J., Winterbourne, J., Czarnota, K. and White, N. 2017. Oceanic residual depth measurements, the plate cooling model, and global dynamic topography. *Journal of Geophysical Research Solid Earth*, **122**, 2328–2372, <https://doi.org/10.1002/2016JB013457>
- Hole, M.J. and LeMasurier, W.E. 1994. Tectonic controls on the geochemical composition of Cenozoic, mafic alkaline volcanic rocks from West Antarctica. *Contributions to Mineralogy and Petrology*, **117**, 187–202, <https://doi.org/10.1007/BF00286842>
- Huerta, A.D. 2007. Byrd drainage system; evidence of a Mesozoic West Antarctic plateau. In: Cooper, A.K. and Raymond, C.R. (eds) *Antarctica: A Keystone in a Changing World – Online Proceedings of the 10th ISAES X*. USGS Open-File Report 2007-1047. Extended Abstract 091.
- Humbert, A., Steinhage, D., Helm, V., Beyer, S. and Kleiner, T. 2018. Missing evidence of Widespread Subglacial Lakes at Recovery Glacier, Antarctica. *Journal of Geophysical Research Earth Surface*, **123**, 2802–2826, <https://doi.org/10.1029/2017JF004591>
- Jamieson, S.S.R. and Sugden, D.E. 2008. Landscape evolution of Antarctica. In: Cooper, A.K., Barrett, P.J., Stagg, H., Storey, B., Stump, E. and Wise, W. (eds) *Antarctica: A Keystone in a Changing World*. The National Academies Press, Washington DC, 39–54, <https://doi.org/10.1007/s13398-014-0173-7.2>
- Jamieson, S.S.R., Hulton, N.R.J., Sugden, D.E., Payne, A.J. and Taylor, J. 2005. Cenozoic landscape evolution of the Lambert basin, East Antarctica: the relative role of rivers and ice sheets. *Global and Planetary Change*, **45**, 35–49, <https://doi.org/10.1016/j.gloplacha.2004.09.015>
- Jamieson, S.S.R., Hulton, N.R.J. and Hagdorn, M. 2008. Modelling landscape evolution under ice sheets. *Geomorphology*, **97**, 91–108, <https://doi.org/10.1016/j.geomorph.2007.02.047>
- Jamieson, S.S.R., Sugden, D.E. and Hulton, N.R.J. 2010. The evolution of the subglacial landscape of Antarctica. *Earth and Planetary Science Letters*, **293**, 1–27, <https://doi.org/10.1016/j.epsl.2010.02.012>
- Jamieson, S.S.R., Stokes, C.R. *et al.* 2014. The glacial geomorphology of the Antarctic ice sheet bed. *Antarctic Science*, **26**, 724–741, <https://doi.org/10.1017/S0954102014000212>
- Japsen, P., Bonow, J.M., Green, P.F., Chalmers, J.A. and Lidmar-Bergström, K. 2006. Elevated, passive continental margins: long-term highs or Neogene uplifts? New evidence from West Greenland. *Earth and Planetary Science Letters*, **248**, 330–339, <https://doi.org/10.1016/j.epsl.2006.05.036>
- Ji, F., Gao, J., Shen, Z., Zhang, Q. and Li, Y. 2017. Variations of the effective elastic thickness over the Ross Sea and Transantarctic Mountains and implications for their structure and tectonics. *Tectonophysics*, **717**, 127–138, <https://doi.org/10.1016/j.tecto.2017.07.011>
- Jordan, T.A., Ferraccioli, F., Vaughan, D.G., Holt, J.W., Corr, H., Blankenship, D.D. and Diehl, T.M., 2010. Aerogravity evidence for major crustal thinning under the Pine Island Glacier region (West Antarctica). *Geological Society of America Bulletin*, **122**, 714–726, <https://doi.org/10.1130/B26417.1>
- Jordan, T.A., Ferraccioli, F., Armadillo, E. and Bozzo, E. 2013. Crustal architecture of the Wilkes Subglacial Basin in East Antarctica, as revealed from airborne gravity data. *Tectonophysics*, **585**, 196–206, <https://doi.org/10.1016/j.tecto.2012.06.041>
- Jordan, T.A., Ferraccioli, F. and Leat, P.T. 2017. New geophysical compilations link crustal block motion to Jurassic extension and strike-slip faulting in the Weddell Sea Rift System of West Antarctica. *Gondwana Research*, **42**, 29–48, <https://doi.org/10.1016/j.gr.2016.09.009>
- Jordan, T.A., Martin, C. *et al.* 2018. Anomalously high geothermal flux near the South Pole. *Scientific Reports*, **8**, 16785, <https://doi.org/10.1038/s41598-018-35182-0>
- Joughin, I. and Alley, R.B. 2011. Stability of the West Antarctic ice sheet in a warming world. *Nature Geoscience*, **4**, 506–513, <https://doi.org/10.1038/ngeo1194>
- Karlsson, N.B., Binder, T., Eagles, G., Helm, V., Pattyn, F., Van Liefferinge, B. and Eisen, O. 2018. Glaciological characteristics in the Dome Fuji region and new assessment for ‘Oldest Ice’. *Cryosphere*, **12**, 2413–2424, <https://doi.org/10.5194/tc-12-2413-2018>
- Karner, G.D., Studinger, M. and Bell, R.E. 2005. Gravity anomalies of intermediary basins and their mechanical implications: application to the Ross Sea basins, West Antarctica. *Earth and Planetary Science Letters*, **235**, 577–596, <https://doi.org/10.1016/j.epsl.2005.04.016>
- Katz, M.E., Miller, K.G., Wright, J.D., Wade, B.S., Browning, J.V., Cramer, B.S. and Rosenthal, Y. 2008. Stepwise transition from the Eocene greenhouse to the Oligocene icehouse. *Nature Geoscience*, **1**, 329–334, <https://doi.org/10.1038/ngeo1179>
- Kennett, J.P. 1977. Cenozoic evolution of Antarctic glaciation, the circum-Antarctic Ocean, and their impact on global paleoceanography. *Journal of Geophysical Research*, **82**, 3843–3860, <https://doi.org/10.1029/JC082i027p03843>
- Kessler, M.A., Anderson, R.S. and Briner, J.P. 2008. Fjord insertion into continental margins driven by topographic steering of ice. *Nature Geoscience*, **1**, 365–369, <https://doi.org/10.1038/ngeo201>
- Kingslake, J., Scherer, R.P. *et al.* 2018. Extensive retreat and re-advance of the West Antarctic Ice Sheet during the Holocene. *Nature*, **558**, 430–434, <https://doi.org/10.1038/s41586-018-0208-x>
- Kirby, J.F. 2014. Estimation of the effective elastic thickness of the lithosphere using inverse spectral methods: the state of the art. *Tectonophysics*, **631**, 87–116, <https://doi.org/10.1016/j.tecto.2014.04.021>
- Koppes, M.N. and Montgomery, D.R. 2009. The relative efficacy of fluvial and glacial erosion over modern to orogenic timescales. *Nature Geoscience*, **2**, 644–647, <https://doi.org/10.1038/ngeo616>
- Krohne, N., Lisker, F., Kleinschmidt, G., Klugel, A., Laufer, A., Estrada, S. and Spiegel, C. 2016. The Shackleton Range (East Antarctica): an alien block at the rim of Gondwana? *Geological Magazine*, **155**, 841–864, <https://doi.org/10.1017/S0016756816001011>
- Kulhanek, D.K., Levy, R.H. *et al.* 2019. Revised chronostratigraphy of DSDP Site 270 and late Oligocene to early Miocene paleoecology of the Ross Sea sector of Antarctica. *Global and Planetary Change*, **178**, 46–64, <https://doi.org/10.1016/j.gloplacha.2019.04.002>
- Lawrence, J.F., Wiens, D.A., Nyblade, A.A., Anandkrishnan, S., Shore, P.J. and Voigt, D. 2006. Crust and upper mantle structure of the Transantarctic Mountains and surrounding regions from

## Antarctic palaeotopography

- receiver functions, surface waves, and gravity: implications for uplift models. *Geochemistry, Geophysics Geosystems*, **7**, <https://doi.org/10.1029/2006GC001282>
- Leckie, R.M. and Webb, P.-N. 1983. Late Oligocene-early Miocene glacial record of the Ross Sea, Antarctica: evidence from DSDP Site 270. *Geology*, **11**, 578–582, [https://doi.org/10.1130/0091-7613\(1983\)11<578:LOMGRO>2.0.CO;2](https://doi.org/10.1130/0091-7613(1983)11<578:LOMGRO>2.0.CO;2)
- LeMasurier, W.E. and Landis, C.A. 1996. Mantle-plume activity recorded by low-relief erosion surfaces in West Antarctica and New Zealand. *Geological Society of America Bulletin*, **108**, 1450–1466, [https://doi.org/10.1130/0016-7606\(1996\)108<1450:MPARBL>2.3.CO;2](https://doi.org/10.1130/0016-7606(1996)108<1450:MPARBL>2.3.CO;2)
- LeMasurier, W.E. and Rex, D.C. 1989. Evolution of linear volcanic ranges in Marie Byrd Land, West Antarctica. *Journal of Geophysical Research*, **94**, 7223, <https://doi.org/10.1029/JB094iB06p07223>
- LeMasurier, W.E., Thomson, J.W., Baker, P.E., Kyle, P.R., Rowley, P.D., Smellie, J.L. and Verwoerd, W.J. (eds) 1990. *Volcanoes of the Antarctic Plate and Southern Oceans*. American Geophysical Union, *Antarctic Research Series*, Washington, DC, <https://doi.org/10.1029/AR048>
- Leuschen, C., Gogineni, P., Rodriguez-Morales, F., Paden, J. and Allen, C. 2016. *IceBridge MCoRDS L2 Ice Thickness, Version 1*. NASA National Snow and Ice Data Center Distributed Active Archive Center, Boulder, Colorado, USA.
- Liu, Z., Pagani, M. *et al.* 2009. Global cooling during the Eocene–Oligocene climate transition. *Science*, **323**, 1187–1190, <https://doi.org/10.1126/science.1166368>
- Lloyd, A.J., Wiens, D.A. *et al.* 2015. A seismic transect across West Antarctica: evidence for mantle thermal anomalies beneath the Bentley Subglacial Trench and the Marie Byrd Land Dome. *Journal of Geophysical Research Solid Earth*, **120**, 8439–8460, <https://doi.org/10.1002/2015JB012455>
- Lloyd, A.J., Wiens, D.A. *et al.* 2020. Seismic structure of the Antarctic upper mantle imaged with adjoint tomography. *Journal of Geophysical Research Solid Earth*, **125**, 2019JB017823, <https://doi.org/10.1029/2019JB017823>
- Lythe, M., Vaughan, D.G. *et al.* 2001. BEDMAP: a new ice thickness and subglacial topographic model of Antarctica. *Journal of Geophysical Research*, **106**, 11335–11351, <https://doi.org/10.1029/2000JB900449>
- Maritati, A., Aitken, A.R.A., Young, D.A., Roberts, J.L., Blankenship, D.D. and Siegert, M.J. 2016. The tectonic development and erosion of the Knox Subglacial Sedimentary Basin, East Antarctica. *Geophysical Research Letters*, **43**, 10728–10737, <https://doi.org/10.1002/2016GL071063>
- McKenzie, D. 1978. Some remarks on development of sedimentary basins. *Earth and Planetary Science Letters*, **40**, 25–32, [https://doi.org/10.1016/0012-821x\(78\)90071-7](https://doi.org/10.1016/0012-821x(78)90071-7)
- McKenzie, D. 1994. *The Relationship between Topography and Gravity on Earth and Venus*. *Icarus*, <https://doi.org/10.1006/icar.1994.1170>
- McKenzie, D. 2010. The influence of dynamically supported topography on estimates of Te. *Earth and Planetary Science Letters*, **295**, 127–138, <https://doi.org/10.1016/j.epsl.2010.03.033>
- McKenzie, D. and Fairhead, D. 1997. Estimates of the effective elastic thickness of the continental lithosphere from Bouguer and free air gravity anomalies. *Journal of Geophysical Research*, **102**, 27523–27552, <https://doi.org/10.1029/97JB02481>
- McKenzie, D.P., Roberts, J.M. and Weiss, N.O. 1974. Convection in the earth's mantle: towards a numerical simulation. *Journal of Fluid Mechanics*, **62**, 465–538, <https://doi.org/10.1017/S0022112074000784>
- Menard, H.W. 1973. Depth anomalies and the bobbing motion of drifting islands. *Journal of Geophysical Research*, **78**, 5128–5137, <https://doi.org/10.1029/jb078i023p05128>
- Mengel, M. and Levermann, A. 2014. Ice plug prevents irreversible discharge from East Antarctica. *Nature Climate Change*, **4**, 451–455, <https://doi.org/10.1038/nclimate2226>
- Mercer, J.H. 1978. West Antarctic ice sheet and CO<sub>2</sub> greenhouse effect: a threat of disaster. *Nature*, **271**, 321–325, <https://doi.org/10.1073/pnas.0703993104>
- Molnar, P. and England, P. 1990. Late Cenozoic uplift of mountain ranges and global climate change: chicken or egg? *Nature*, **346**, 29–34, <https://doi.org/10.1038/346029a0>
- Molnar, P., England, P.C. and Jones, C.H. 2015. Mantle dynamics, isostasy, and the support of high terrain. *Journal of Geophysical Research Solid Earth*, **120**, 1–26, <https://doi.org/10.1002/2014JB011724>
- Morlighem, M., Rignot, E. *et al.* 2020. Deep glacial troughs and stabilizing ridges unveiled beneath the margins of the Antarctic ice sheet. *Nature Geoscience*, **13**, 132–137, <https://doi.org/10.1038/s41561-019-0510-8>
- Müller, R.D., Seton, M. *et al.* 2016. Ocean basin evolution and global-scale plate reorganization events since Pangea breakup. *Annual Review of Earth and Planetary Science*, **44**, 107–138, <https://doi.org/10.1146/annurev-earth-060115-012211>
- Naish, T.R., Woolfe, K.J. *et al.* 2001. Orbitally induced oscillations in the East Antarctic ice sheet at the Oligocene/Miocene boundary. *Nature*, **413**, 719–723, <https://doi.org/10.1038/35099534>
- O'Donnell, J.P. and Nyblade, A.A. 2014. Antarctica's hypsometry and crustal thickness: Implications for the origin of anomalous topography in East Antarctica. *Earth and Planetary Science Letters*, **388**, 143–155, <https://doi.org/10.1016/j.epsl.2013.11.051>
- Olivetti, V., Rossetti, F., Balestrieri, M.L., Pace, D., Cornamusini, G. and Talarico, F. 2018. Variability in uplift, exhumation and crustal deformation along the Transantarctic Mountains front in southern Victoria Land, Antarctica. *Tectonophysics*, **745**, 229–244, <https://doi.org/10.1016/j.tecto.2018.08.017>
- Pagani, M., Huber, M. *et al.* 2011. The role of carbon dioxide during the onset of Antarctic glaciation. *Science*, **334**, 1261–1264, <https://doi.org/10.1126/science.1203909>
- Pappa, F. and Ebbing, J. 2021. Gravity, magnetics and geothermal heat flow of the Antarctic lithospheric crust and mantle. *Geological Society, London, Memoirs*, **56**, <https://doi.org/10.1144/M56-2020-5>
- Pappa, F., Ebbing, J. and Ferraccioli, F. 2019. Moho depths of Antarctica: comparison of seismic, gravity, and isostatic results. *Geochemistry, Geophysics, Geosystems*, **20**, 1629–1645, <https://doi.org/10.1029/2018GC008111>
- Passchier, S., Ciarletta, D.J., Miriagos, T.E., Bijl, P.K. and Bohaty, S.M. 2017. An Antarctic stratigraphic record of stepwise ice growth through the Eocene–Oligocene transition. *Geological Society of America Bulletin*, **129**, 318–330, <https://doi.org/10.1130/B31482.1>
- Paxman, G.J.G., Watts, A.B., Ferraccioli, F., Jordan, T.A., Bell, R.E., Jamieson, S.S.R. and Finn, C.A. 2016. Erosion-driven uplift in the Gamburtsev Subglacial Mountains of East Antarctica. *Earth and Planetary Science Letters*, **452**, 1–14, <https://doi.org/10.1016/j.epsl.2016.07.040>
- Paxman, G.J.G., Jamieson, S.S.R. *et al.* 2017. Uplift and tilting of the Shackleton Range in East Antarctica driven by glacial erosion and normal faulting. *Journal of Geophysical Research Solid Earth*, **122**, 2390–2408, <https://doi.org/10.1002/2016JB013841>
- Paxman, G.J.G., Jamieson, S.S.R. *et al.* 2018. Bedrock erosion surfaces record former East Antarctic Ice Sheet extent. *Geophysical Research Letters*, **45**, 4114–4123, <https://doi.org/10.1029/2018GL077268>
- Paxman, G.J.G., Jamieson, S.S.R. *et al.* 2019a. The role of lithospheric flexure in the landscape evolution of the Wilkes Subglacial Basin and Transantarctic Mountains, East Antarctica. *Journal of Geophysical Research Earth Surface*, **124**, 812–829, <https://doi.org/10.1029/2018JF004705>
- Paxman, G.J.G., Jamieson, S.S.R., Hochmuth, K., Gohl, K., Bentley, M.J., Leitchenkov, G. and Ferraccioli, F. 2019b. Reconstructions of Antarctic topography since the Eocene–Oligocene boundary. *Palaeogeography Palaeoclimatology Palaeoecology*, **535**, 109346, <https://doi.org/10.1016/j.palaeo.2019.109346>
- Paxman, G.J.G., Gasson, E.G.W., Jamieson, S.S.R., Bentley, M.J. and Ferraccioli, F. 2020. Long-term increase in Antarctic Ice Sheet vulnerability driven by bed topography evolution. *Geophysical Research Letters*, **47**.

- Pearson, P.N., Foster, G.L. and Wade, B.S. 2009. Atmospheric carbon dioxide through the Eocene–Oligocene climate transition. *Nature*, **461**, 1110–1113, <https://doi.org/10.1038/nature08447>
- Pekeris, C.L. 1935. Thermal convection in the interior of the earth. *Geophysics Journal International*, **3**, 343–367, <https://doi.org/10.1111/j.1365-246X.1935.tb01742.x>
- Pollard, D. and DeConto, R.M. 2009. Modelling West Antarctic ice sheet growth and collapse through the past five million years. *Nature*, **458**, 329–332, <https://doi.org/10.1038/nature07809>
- Pollard, D. and DeConto, R.M. 2019. Continuous simulations over the last 40 million years with a coupled Antarctic ice sheet–sediment model. *Palaeogeography Palaeoclimatology Palaeoecology*, **537**, 109374, <https://doi.org/10.1016/J.PALAEO.2019.109374>
- Pollard, D., DeConto, R.M. and Alley, R.B. 2015. Potential Antarctic Ice Sheet retreat driven by hydrofracturing and ice cliff failure. *Earth and Planetary Science Letters*, **412**, 112–121, <https://doi.org/10.1016/j.epsl.2014.12.035>
- Quigley, M.C., Clark, D. and Sandiford, M. 2010. Tectonic geomorphology of Australia. *Geological Society, London, Special Publications*, **346**, 243–265, <https://doi.org/10.1144/SP346.13>
- Ramirez, C., Nyblade, A. *et al.* 2016. Crustal and upper-mantle structure beneath ice-covered regions in Antarctica from S-wave receiver functions and implications for heat flow. *Geophysics Journal International*, **204**, 1636–1648, <https://doi.org/10.1093/gji/ggv542>
- Reusch, D.N. 2011. New Caledonian carbon sinks at the onset of Antarctic glaciation. *Geology*, **39**, 807–810, <https://doi.org/10.1130/G31981.1>
- Richards, F.D., Hoggard, M.J. and White, N.J. 2016. Cenozoic epeirogeny of the Indian peninsula. *Geochemistry, Geophysics, Geosystems*, **17**, 4920–4954, <https://doi.org/10.1002/2016GC006545>
- Rignot, E., Bamber, J.L., van den Broeke, M.R., Davis, C., Li, Y., van de Berg, W.J. and van Meijgaard, E. 2008. Recent Antarctic ice mass loss from radar interferometry and regional climate modelling. *Nature Geoscience*, **1**, 106–110, <https://doi.org/10.1038/ngeo102>
- Rocchi, S., Armienti, P., D’Orazio, M., Tonarini, S., Wijbrans, J.R. and Di Vincenzo, G. 2002. Cenozoic magmatism in the western Ross Embayment: role of mantle plume v. plate dynamics in the development of the West Antarctic Rift System. *Journal of Geophysical Research Solid Earth*, **107**, <https://doi.org/10.1029/2001JB000515>
- Rocchi, S., LeMasurier, W.E. and Di Vincenzo, G. 2006. Oligocene to Holocene erosion and glacial history in Marie Byrd Land, West Antarctica, inferred from exhumation of the Dorrel Rock intrusive complex and from volcano morphologies. *Geological Society of America Bulletin*, **118**, 991–1005, <https://doi.org/10.1130/B25675.1>
- Rose, K.C., Ferraccioli, F. *et al.* 2013. Early East Antarctic Ice Sheet growth recorded in the landscape of the Gamburtsev Subglacial Mountains. *Earth and Planetary Science Letters*, **375**, 1–12, <https://doi.org/10.1016/j.epsl.2013.03.053>
- Sandiford, M., Quigley, M., de Broekert, P. and Jakica, S. 2009. Tectonic framework for the Cenozoic cratonic basins of Australia. *Australian Journal of Earth Science*, **56**, S5–S18, <https://doi.org/10.1080/08120090902870764>
- Scheinert, M., Ferraccioli, F. *et al.* 2016. New Antarctic gravity anomaly grid for enhanced geodetic and geophysical studies in Antarctica. *Geophysical Research Letters*, **43**, 600–610, <https://doi.org/10.1002/2015GL067439>
- Scher, H.D., Bohaty, S.M., Zachos, J.C. and Delaney, M.L. 2011. Two-stepping into the icehouse: east Antarctic weathering during progressive ice-sheet expansion at the Eocene–Oligocene transition. *Geology*, **39**, 383–386, <https://doi.org/10.1130/G31726.1>
- Scherer, R.P., Aldahan, A., Tulaczyk, S., Possnert, G., Engelhardt, H. and Kamb, B. 1998. Pleistocene collapse of the west Antarctic ice sheet. *Science*, **281**, 82–85, <https://doi.org/10.1126/science.281.5373.82>
- Schoof, C. 2007. Ice sheet grounding line dynamics: steady states, stability, and hysteresis. *Journal of Geophysical Research*, **112**, F03S28, <https://doi.org/10.1029/2006JF000664>
- Schroeder, D.M., Dowdeswell, J.A. *et al.* 2019. Multidecadal observations of the Antarctic ice sheet from restored analog radar records. *Proceedings of the National Academy of Sciences*, **116**, 18867–18873, <https://doi.org/10.1073/pnas.1821646116>
- Seroussi, H., Ivins, E.R., Wiens, D.A. and Bondzio, J. 2017. Influence of a West Antarctic mantle plume on ice sheet basal conditions. *Journal of Geophysical Research Solid Earth*, **122**, 7127–7155, <https://doi.org/10.1002/2017JB014423>
- Shen, W., Wiens, D.A. *et al.* 2017. Seismic evidence for lithospheric foundering beneath the southern Transantarctic Mountains, Antarctica. *Geology*, **46**, 1–4, <https://doi.org/10.1130/G39555.1>
- Shen, W., Wiens, D.A. *et al.* 2018. The crust and upper mantle structure of central and west Antarctica from Bayesian inversion of Rayleigh wave and receiver functions. *Journal of Geophysical Research Solid Earth*, **123**, 7824–7849, <https://doi.org/10.1029/2017JB015346>
- Siddoway, C.S., Richard, S.M., Fanning, C.M. and Luyendyk, B.P. 2004. Origin and emplacement of a middle Cretaceous gneiss dome, Fosdick Mountains, West Antarctica. *Geological Society of America Special Papers*, **380**, 267–294, <https://doi.org/10.1130/0-8137-2380-9.267>
- Spiegel, C., Lindow, J. *et al.* 2016. Tectonomorphic evolution of Marie Byrd Land – implications for Cenozoic rifting activity and onset of West Antarctic glaciation. *Global and Planetary Change*, **145**, 98–115, <https://doi.org/10.1016/j.gloplacha.2016.08.013>
- Stern, T.A. and ten Brink, U.S. 1989. Flexural uplift of the Transantarctic Mountains. *Journal of Geophysical Research*, **94**, 10315–10330, <https://doi.org/10.1029/JB094iB08p10315>
- Stern, T.A., Baxter, A.K. and Barrett, P.J. 2005. Isostatic rebound due to glacial erosion within the Transantarctic Mountains. *Geology*, **33**, 221–224, <https://doi.org/10.1130/G21068.1>
- Studinger, M. and Miller, H. 1999. Crustal structure of the Filchner-Ronne Shelf and Coats Land, Antarctica, from gravity and magnetic data: implications for the breakup of Gondwana. *Journal of Geophysical Research Solid Earth*, **104**, 20379–20394, <https://doi.org/10.1029/1999JB900117>
- Studinger, M., Bell, R.E., Blankenship, D.D., Finn, C.A., Arko, R.A., Morse, D.L. and Joughin, I. 2001. Subglacial sediments: a regional geological template for ice flow in West Antarctica. *Geophysical Research Letters*, **28**, 3493–3496, <https://doi.org/10.1029/2000GL011788>
- Studinger, M., Bell, R.E., Buck, W.R., Karner, G.D. and Blankenship, D.D. 2004. Sub-ice geology inland of the Transantarctic Mountains in light of new aerogeophysical data. *Earth and Planetary Science Letters*, **220**, 391–408, [https://doi.org/10.1016/S0012-821X\(04\)00066-4](https://doi.org/10.1016/S0012-821X(04)00066-4)
- Stump, E., Sheridan, M.F., Borg, S.G. and Sutter, J.F. 1980. Early miocene subglacial basalts, the east Antarctic ice sheet, and uplift of the Transantarctic Mountains. *Science*, **207**, 757–759, <https://doi.org/10.1126/science.207.4432.757>
- Sugden, D.E. and Denton, G.H. 2004. Cenozoic landscape evolution of the Convoy Range to Mackay Glacier area, Transantarctic Mountains: onshore to offshore synthesis. *Geological Society of America Bulletin*, **116**, 840–857, <https://doi.org/10.1130/B25356.1>
- Sugden, D.E. and Jamieson, S.S.R. 2018. The pre-glacial landscape of Antarctica. *Scottish Geographical Journal*, **134**, 203–223, <https://doi.org/10.1080/14702541.2018.1535090>
- Sugden, D.E. and John, B.S. 1976. *Glaciers and Landscape*. Edward Arnold, London.
- Sutherland, R., Spasojevic, S. and Gurnis, M. 2010. Mantle upwelling after Gondwana subduction death explains anomalous topography and subsidence histories of eastern New Zealand and west Antarctica. *Geology*, **38**, 155–158, <https://doi.org/10.1130/G30613.1>
- Taylor, J., Siegert, M.J., Payne, A.J. and Hubbard, B. 2004. Regional-scale bed roughness beneath ice masses: measurement and analysis. *Computers & Geosciences*, **30**, 899–908, <https://doi.org/10.1016/j.cageo.2004.06.007>

## Antarctic palaeotopography

- ten Brink, U.S., Hackney, R.I., Bannister, S., Stern, T.A. and Makovsky, Y. 1997. Uplift of the Transantarctic Mountains and the bedrock beneath the East Antarctic ice sheet. *Journal of Geophysical Research Solid Earth*, **102**, 27603–27621, <https://doi.org/10.1029/97jb02483>
- Thomas, R.H. 1979. The dynamics of marine ice sheets. *Journal of Glaciology*, **24**, 167–177, <https://doi.org/10.1017/S0022143000014726>
- Thomson, S.N., Reiners, P.W., Hemming, S.R. and Gehrels, G.E. 2013. The contribution of glacial erosion to shaping the hidden landscape of East Antarctica. *Nature Geoscience*, **6**, 203–207, <https://doi.org/10.1038/ngeo1722>
- Tinto, K.J., Padman, L. *et al.* 2019. Ross Ice Shelf response to climate driven by the tectonic imprint on seafloor bathymetry. *Nature Geoscience*, **12**, 441–449, <https://doi.org/10.1038/s41561-019-0370-2>
- Tochilin, C.J., Reiners, P.W., Thomson, S.N., Gehrels, G.E., Hemming, S.R. and Pierce, E.L. 2012. Erosional history of the Prydz Bay sector of East Antarctica from detrital apatite and zircon geo- and thermochronology multidating. *Geochemistry, Geophysics, Geosystems*, **13**, 1–21, <https://doi.org/10.1029/2012GC004364>
- Tripati, A., Backman, J., Elderfield, H. and Ferretti, P. 2005. Eocene bipolar glaciation associated with global carbon cycle changes. *Nature*, **436**, 341–346, <https://doi.org/10.1038/nature04289>
- van Wijk, J.W., Lawrence, J.F. and Driscoll, N.W. 2008. Formation of the Transantarctic Mountains related to extension of the West Antarctic Rift system. *Tectonophysics*, **458**, 117–126, <https://doi.org/10.1016/j.tecto.2008.03.009>
- van Wyk de Vries, M., Bingham, R.G. and Hein, A.S. 2018. A new volcanic province: an inventory of subglacial volcanoes in West Antarctica. *Geological Society, London, Special Publications*, **461**, 231–248, <https://doi.org/10.1144/SP461.7>
- Watts, A.B. 2001. *Isostasy and Flexure of the Lithosphere*. Cambridge University Press, Cambridge.
- Watts, A.B. and Burov, E.B. 2003. Lithospheric strength and its relationship to the elastic and seismogenic layer thickness. *Earth and Planetary Science Letters*, **213**, 113–131, [https://doi.org/10.1016/S0012-821X\(03\)00289-9](https://doi.org/10.1016/S0012-821X(03)00289-9)
- Watts, A.B. and Moore, J.D.P. 2017. Flexural isostasy: constraints from gravity and topography power spectra. *Journal of Geophysical Research Solid Earth*, **122**, 1–14, <https://doi.org/10.1002/2017JB014571>
- Watts, A.B., Zhong, S.J. and Hunter, J. 2013. The behavior of the lithosphere on seismic to geologic timescales. *Annual Review of Earth and Planetary Science*, **41**, 443–468, <https://doi.org/10.1146/annurev-earth-042711-105457>
- Weissel, J.K. and Karner, G.D. 1989. Flexural uplift of rift flanks due to mechanical unloading of the lithosphere during extension. *Journal of Geophysical Research Solid Earth*, **94**, 13919–13950, <https://doi.org/10.1029/JB094iB10p13919>
- Wenman, C.P., Harry, D.L. and Jha, S. 2020. Post middle Miocene tectonomagmatic and stratigraphic evolution of the Victoria Land Basin, West Antarctica. *Geochemistry, Geophysics, Geosystems*, **21**, <https://doi.org/10.1029/2019GC008568>
- White, D.A. 2013. Cenozoic landscape and ice drainage evolution in the Lambert Glacier-Amery Ice Shelf system. *Geological Society, London, Special Publications*, **381**, 151–165, <https://doi.org/10.1144/SP381.15>
- Whittaker, J.M., Müller, R.D. and Gurnis, M. 2010. Development of the Australian–Antarctic depth anomaly. *Geochemistry, Geophysics, Geosystems*, **11**, <https://doi.org/10.1029/2010GC003276>
- Wiens, D.A., Shen, W. and Lloyd, A. 2021. The seismic structure of the Antarctic upper mantle. *Geological Society, London, Memoirs*, **56**, <https://doi.org/10.1144/M56-2020-18>
- Wilson, D.S. and Luyendyk, B.P. 2006. Bedrock platforms within the Ross Embayment, West Antarctica: hypotheses for ice sheet history, wave erosion, Cenozoic extension, and thermal subsidence. *Geochemistry, Geophysics Geosystems*, **7**, 1–23, <https://doi.org/10.1029/2006GC001294>
- Wilson, D.S. and Luyendyk, B.P. 2009. West Antarctic paleotopography estimated at the Eocene–Oligocene climate transition. *Geophysical Research Letters*, **36**, L16302, <https://doi.org/10.1029/2009GL039297>
- Wilson, D.S., Jamieson, S.S.R., Barrett, P.J., Leitchenkov, G., Gohl, K. and Larter, R.D. 2012. Antarctic topography at the Eocene–Oligocene boundary. *Palaeogeography Palaeoclimatology Palaeoecology*, **335–336**, 24–34, <https://doi.org/10.1016/j.palaeo.2011.05.028>
- Wilson, D.S., Pollard, D., DeConto, R.M., Jamieson, S.S.R. and Luyendyk, B.P. 2013. Initiation of the West Antarctic Ice Sheet and estimates of total Antarctic ice volume in the earliest Oligocene. *Geophysical Research Letters*, **40**, 4305–4309, <https://doi.org/10.1002/grl.50797>
- Winberry, J.P. and Anandakrishnan, S. 2004. Crustal structure of the West Antarctic rift system and Marie Byrd Land hotspot. *Geology*, **32**, 977–980, <https://doi.org/10.1130/G20768.1>
- Winterbourne, J., White, N. and Crosby, A. 2014. Accurate measurements of residual topography from the oceanic realm. *Tectonics*, **33**, 982–1015, <https://doi.org/10.1002/2013TC003372>
- Young, D.A., Wright, A.P. *et al.* 2011. A dynamic early East Antarctic Ice Sheet suggested by ice-covered fjord landscapes. *Nature*, **474**, 72–75, <https://doi.org/10.1038/nature10114>
- Zachos, J. and Kump, L. 2005. Carbon cycle feedbacks and the initiation of Antarctic glaciation in the earliest Oligocene. *Global and Planetary Change*, **47**, 51–66, <https://doi.org/10.1016/j.gloplacha.2005.01.001>
- Zachos, J.C., Flower, B.P. and Paul, H. 1997. Orbitally paced climate oscillations across the Oligocene/Miocene boundary. *Nature*, **388**, 567–570, <https://doi.org/10.1038/41528>
- Zachos, J., Pagani, M., Sloan, L., Thomas, E. and Billups, K. 2001. Trends, rhythms, and aberrations in global climate 65 Ma to present. *Science*, **292**, 686–693, <https://doi.org/10.1126/science.1059412>
- Zachos, J.C., Dickens, G.R. and Zeebe, R.E. 2008. An early Cenozoic perspective on greenhouse warming and carbon-cycle dynamics. *Nature*, **451**, 279–283, <https://doi.org/10.1038/nature06588>